NATIONAL AERONAUTICS AND SPACE ADMINISTRATION

Technical Report 32-1572

Gain Calibration of a Horn Antenna Using Pattern Integration

A. Ludwig
J. Hardy
R. Norman

JET PROPULSION LABORATORY
CALIFORNIA INSTITUTE OF TECHNOLOGY
PASADENA, CALIFORNIA

October 1, 1972

NATIONAL AERONAUTICS AND SPACE ADMINISTRATION

Technical Report 32-1572

Gain Calibration of a Horn Antenna Using Pattern Integration

A. Ludwig
J. Hardy
R. Norman

JET PROPULSION LABORATORY
CALIFORNIA INSTITUTE OF TECHNOLOGY
PASADENA, CALIFORNIA

October 1, 1972

Preface

The work described in this report was performed by the *Telecommunications* Division of the Jet Propulsion Laboratory.

Acknowledgment

The authors are indebted to Allen Newell, David Kerns, Ronald Bowman, and R. C. Baird for their measurements, which are referred to frequently in this report and which contribute substantially to its content. Dan Bathker provided valuable suggestions and support. Howard Ramsey, Forrest Holdcraft, and Hal Marlin were largely responsible for the excellent accuracy of the antenna range and the digital antenna pattern recording system. Richard Holland developed a portion of the software used in the data reduction and performed measurements similar to those reported here which helped in identifying and minimizing error sources.

Contents

Contents (contd)

Tables

Figures

Abstract

A cooperative program between the Jet Propulsion Laboratory and the National Bureau of Standards will result in the gain measurement of a horn antenna using three different techniques: a two-antenna insertion loss measurement, a pattern integration method, and a near-field measurement method. This article describes the application of the pattern integration method and also the evaluation of the near-field gain correction factors for the horn, which are determined by a new method based directly on measured data. The method involves a spherical wave expansion of the experimental radiation pattern of the specific antenna being tested, rather than evaluation of an assumed analytical model. The spherical wave expansion is also compared to experimental near-field pattern data.

The gain of the antenna is determined by the pattern integration method to be 22.02 dB within a 3σ tolerance (or 99.7% confidence interval) of ± 0.1 dB. It is concluded that the pattern integration method is a valuable technique with a potential of even better accuracies with further development.

Gain Calibration of a Horn Antenna Using Pattern Integration

I. Introduction

The accurate determination of the gain of an antenna is a basic and continuing problem in antenna engineering (Ref. 1). Although the fundamental principles are simple, there are several second-order effects which are complex and difficult to cope with both experimentally and theoretically. These second-order effects generally become significant when accuracies better than roughly $\pm\frac{1}{2}$ dB are required.

There are several motivations for improving the current state-of-the-art in gain measurement techniques: for one, the study is in itself interesting, and involves theoretical and experimental techniques of value in themselves; also, in very expensive communications systems, such as the NASA/JPL Deep Space Network or satellite communication systems, more precise measurements become economically necessary; finally, the experience gained in a precision gain measurement carries over to improve the accuracy of less rigorous measurements.

For these reasons, the basic objective of the work described here is to advance the technology by improving old techniques and evaluating new techniques of precision gain measurements. A second objective is the precision calibration of a JPL gain standard horn. The approach involves a cooperative program between the Jet Propulsion Laboratory (JPL) and the National Bureau of Standards (NBS), in which the gain of a specific JPL horn antenna is determined using three methods: (1) the two-antenna method, in which the "insertion loss" of the link between two identical antennas is measured (Ref. 1); (2) the pattern integration method, in which antenna directivity is directly obtained from the radiation pattern of the antenna (Ref. 2), and (3) a near-field method in which the amplitude and phase of the radiated fields are measured very close to the antenna and then mathematically transformed to yield the far-field pattern and directivity (Ref. 3).

The insertion loss and near-field methods are being applied to the horn by NBS and will be reported separately. This report deals primarily with the pattern integration method, except that the near-field correction factors obtained in the insertion loss method are also obtained here, using a new technique based on the measured antenna patterns.

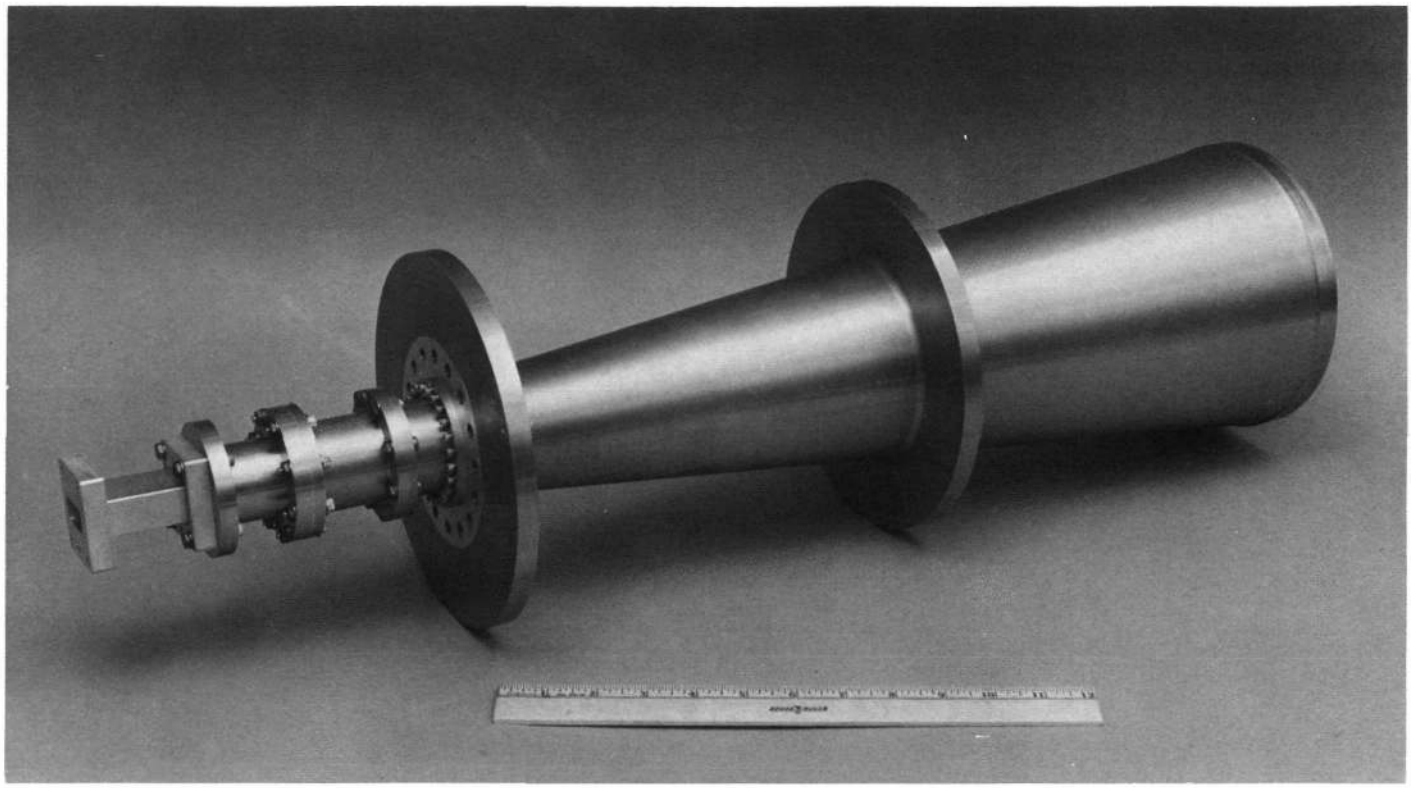

Fig. 1. JPL gain standard horn

The X-band horn antenna selected for calibration as a gain standard is shown in Fig. 1. A linearly polarized circular horn was chosen to take advantage of the minimum pattern data required, as described in the following section. A dual-mode horn (Ref. 4) was chosen because of the very low sidelobes, which have advantages in both calibrating, and using, the horn as a gain standard, such as the minimal ground-bounce multipath shown in a later section. The only possible disadvantage of this horn is its narrow bandwidth. That is, its pattern characteristics and gain change rapidly with frequency. This also makes the horn sensitive to mechanical tolerances, which must be held as close as ± 0.05 mm in critical regions such as the mode-generating section. However, the patterns remain essentially unchanged over a 5% bandwidth, and this is not a problem for the intended application. Detailed mechanical drawings of this horn are available which include the required tolerance specifications (Ref. 5).

II. Pattern Integration Method of Gain Measurement

In this section, the pattern integration method of gain measurement is described, and the basic equations used in this report are presented.

A. Definition of Gain

The basic definition of antenna gain is (Ref. 6)

$$G = \frac{P_0}{P_t/4\pi} \tag{1}$$

where P_0 is the radiation intensity in the direction of interest in watts/steradian, and P_t is total input power for "power" gain or total radiated power for "directive" gain. These two gain definitions differ by the dissipative loss of the antenna itself. For the horn antenna considered here, this loss is small but is included in the final gain calculation presented in a later section.

The basic feature of the pattern integration technique is that the total radiated power is determined relative to the peak of the beam by integrating the pattern radiation intensity, which must include both normal and cross-polarization components; then the directive gain is given by (Ref. 7)

$$G = \frac{4\pi \cdot |\mathbf{E}(0,\phi)|^2}{\int_{\phi=0}^{2\pi} \int_{\theta=0}^{\pi} |\mathbf{E}(\theta,\phi)|^2 \sin\theta \, d\theta \, d\phi} \tag{2}$$

where the coordinate system is shown in Fig. 2.

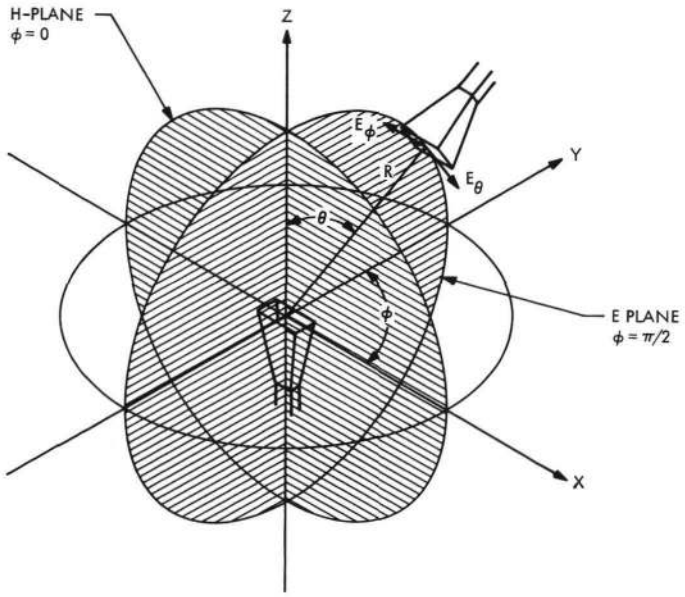

Fig. 2. Antenna pattern coordinates

B. Pattern Symmetry for Circular Horns

In general, it is difficult and time-consuming to experimentally determine $\mathbf{E}(\theta,\phi)$ over a complete sphere; however, in the particular case of a horn with circular symmetry it is only necessary to determine $\mathbf{E}(\theta,\phi)$ for two values of ϕ (Ref. 2). This is due to the fact that a circular horn excited with a field linearly polarized in the y-direction must have a radiation pattern of the form (Ref. 8)

$$\mathbf{E}(\theta,\phi) = E_\theta(\theta) \sin\phi\, \hat{\mathbf{i}}_\theta + E_\phi(\theta) \cos\phi\, \hat{\mathbf{i}}_\phi \tag{3}$$

This is a result of basic symmetry conditions and the form of circular (or conical) waveguide mode fields. Note that this condition does *not* apply to rectangular horns (which are shown in Fig. 2 for illustrative purposes only).

We will now consider the relationship between Eq. (3) and real-world experimental patterns, in order to see what data are required to specify the required functions $E_\theta(\theta)$ and $E_\phi(\phi)$ and also to develop some checks to verify that the actual horn pattern is of this form.

With reference to Fig. 2, the usual method of measuring antenna patterns is to first align the antennas at $\theta = 0$ such that the polarization of the two antennas is matched, for a principal polarization pattern $P(\theta)$, or orthogonal, for a cross-polarized pattern $X(\theta)$. Then the test antenna is rotated in θ, with a fixed orientation of the test antenna in the plane of rotation. After some study, it may be determined that what this measures are patterns given by[1]

$$\begin{aligned} P_{\phi=\phi_0}(\theta) &= \mathbf{E}(\theta,\phi_0) \cdot (\sin\phi_0\, \hat{\mathbf{i}}_\theta + \cos\phi_0\, \hat{\mathbf{i}}_\phi) \\ X_{\phi=\phi_0}(\theta) &= \mathbf{E}(\theta,\phi_0) \cdot (\cos\phi_0\, \hat{\mathbf{i}}_\theta - \sin\phi_0\, \hat{\mathbf{i}}_\phi) \end{aligned} \tag{4}$$

When the antenna radiation pattern $\mathbf{E}(\theta,\phi)$ is of the form of Eq. (3), the measured principal and cross-polarization patterns $P(\theta)$ and $X(\theta)$ are related to this functional form by

$$\begin{aligned} P_{\phi=\phi_0}(\theta) &= E_\theta(\theta) \sin^2\phi_0 + E_\phi(\theta) \cos^2\phi_0 \\ X_{\phi=\phi_0}(\theta) &= [E_\theta(\theta) - E_\phi(\theta)] \sin\phi_0 \cos\phi_0 \end{aligned} \tag{5}$$

Therefore, the measured principal polarization E-plane pattern $P_{\phi=\pi/2}(\theta)$ is identically equal to $E_\theta(\theta)$, and the principal polarization H-plane pattern $P_{\phi=0}(\theta)$ is identically equal to $E_\phi(\theta)$. So these two measured patterns provide precisely the data needed to use Eq. (3) to determine the total antenna pattern, and will be the basic data used in this report. It is important to note that these pattern functions are complex valued, and that both amplitude and phase data are required. Figure 3 shows these patterns for the JPL gain standard horn considered in this report.

It is at first surprising that two principal polarization patterns are sufficient to determine the entire pattern, including cross-polarization, at any cut on the sphere. However, there is a convincing test to verify that this is indeed true. From Eq. (5) the principal and cross-polarized experimental patterns at $\phi = \pi/4$ will be given by

$$\begin{aligned} P_{\phi=\pi/4}(\theta) &= \frac{1}{2}\,[E_\theta(\theta) + E_\phi(\theta)] \\ X_{\phi=\pi/4}(\theta) &= \frac{1}{2}\,[E_\theta(\theta) - E_\phi(\theta)] \end{aligned} \tag{6}$$

It is easy to experimentally measure the two patterns $P(\theta)$ and $X(\theta)$ at $\phi = \pi/4$. These two patterns may also be computed from the E- and H-plane data $E_\theta(\theta)$ and

[1]These patterns are defined as they are usually measured, and there are some peculiarities in the definition. For example, in the $\phi = \pi/4$ plane, the "principal polarization" starts out as E_Y at $\theta = 0$ but ends up as $-E_X$ at $\theta = \pi$. This may violate the intuitive definition of principal polarization but does not cause any problems mathematically.

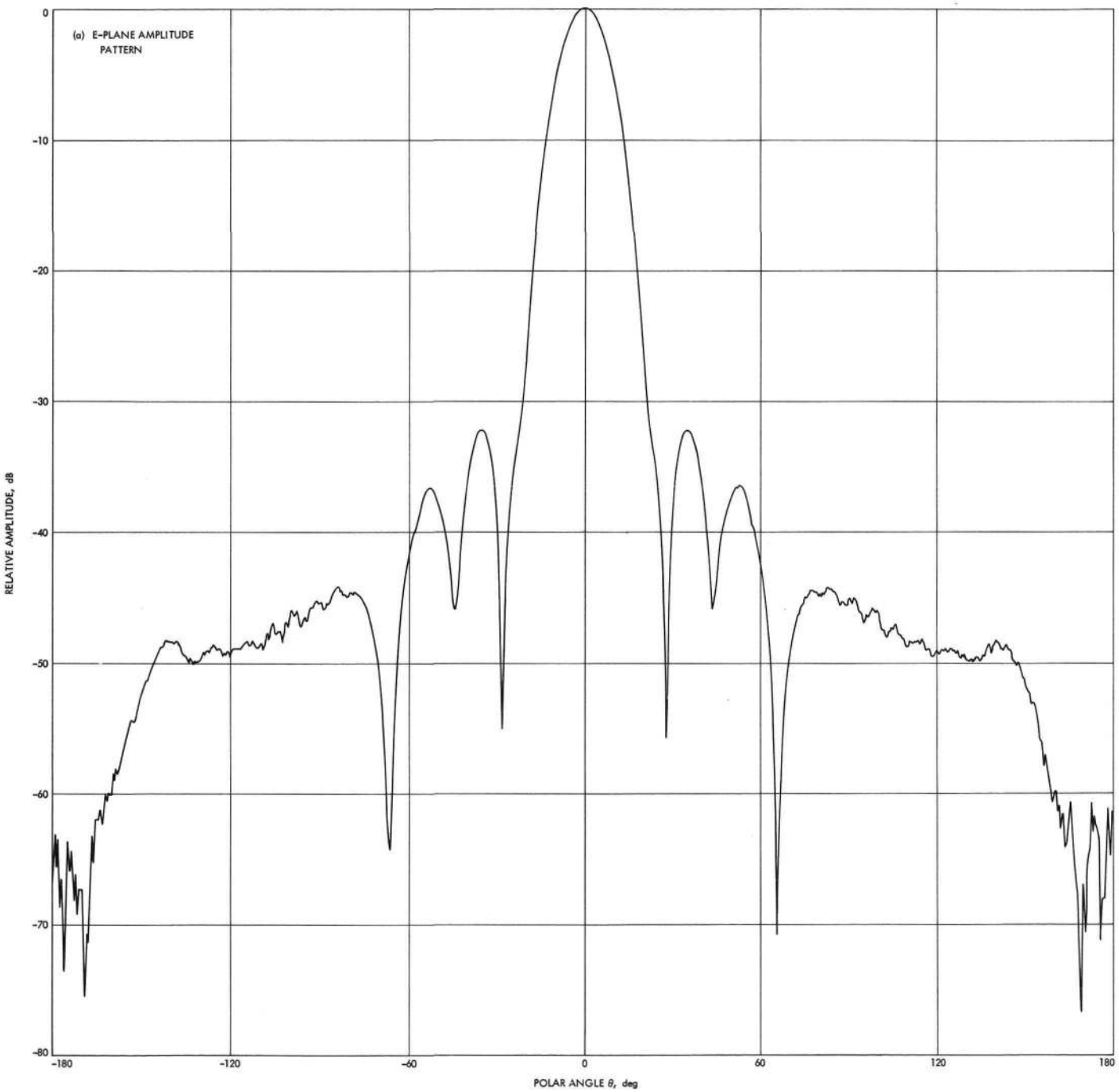

Fig. 3. Patterns of horn antenna

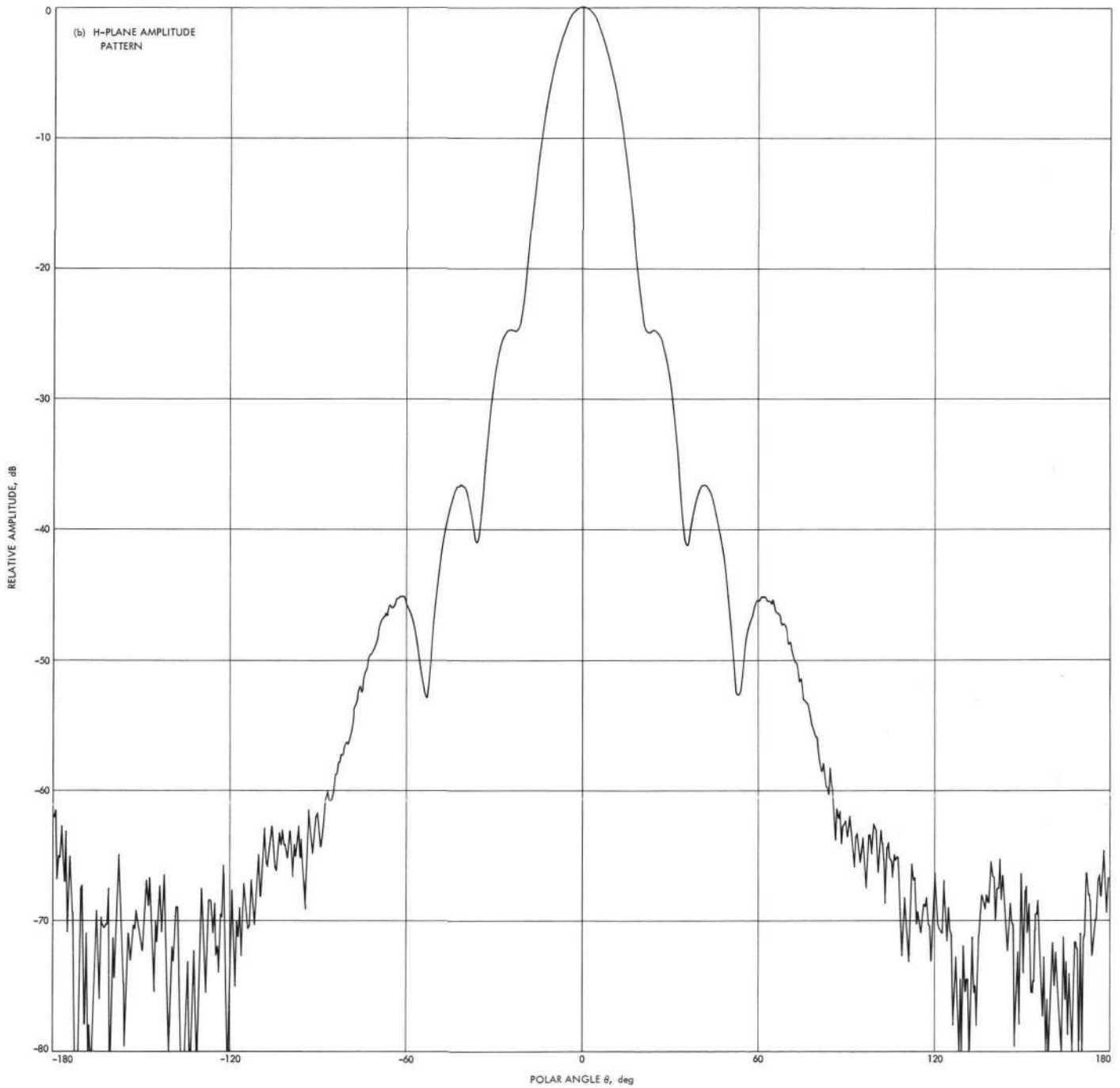
(b) H-PLANE AMPLITUDE PATTERN
0
-10
-20
-30
-40
-50
-60
-70
-80
RELATIVE AMPLITUDE, dB
-180
-120
-60
0
60
120
180
POLAR ANGLE θ, deg

Fig. 3 (contd)

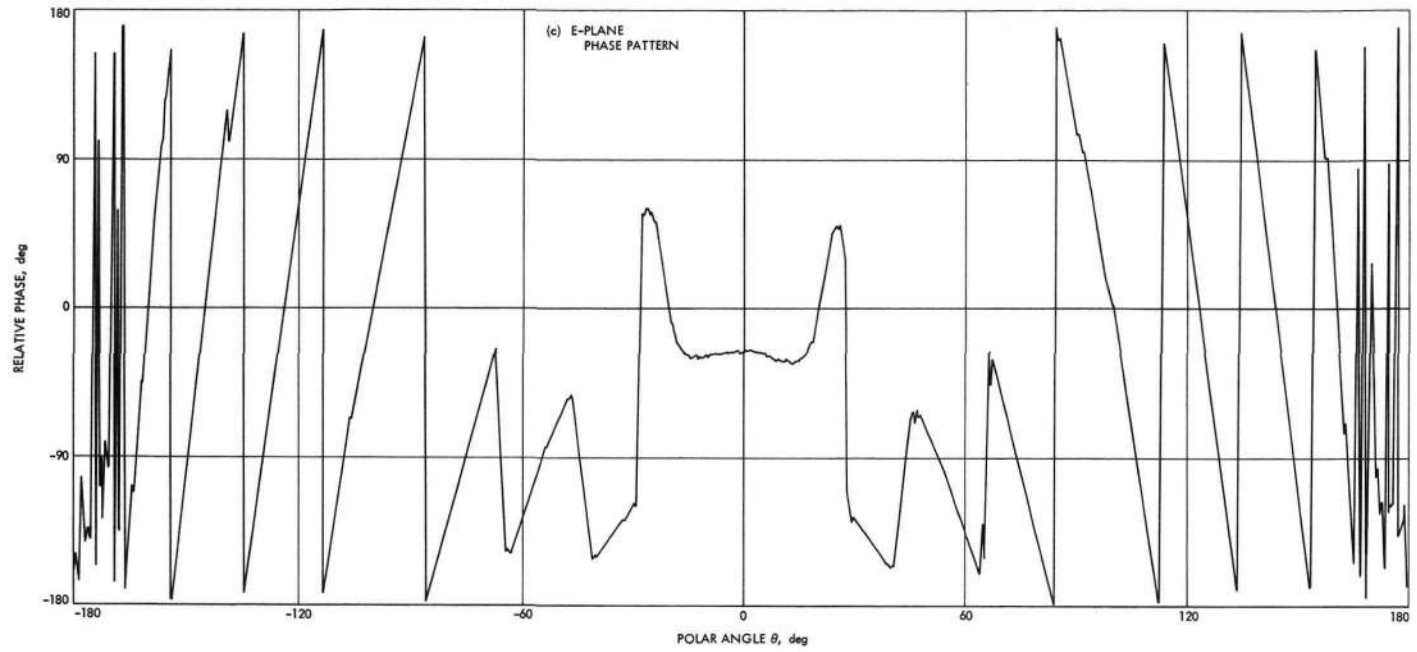

Fig. 3 (contd)

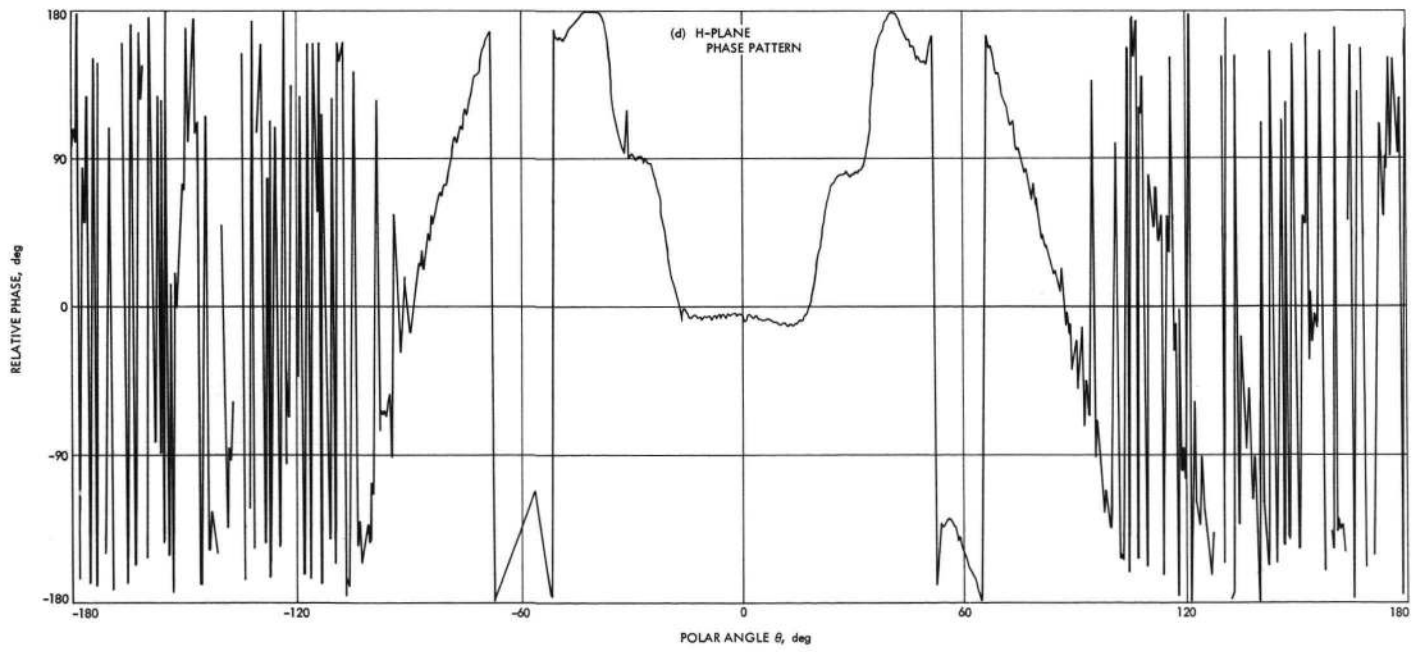

Fig. 3 (contd)

$E_\phi(\theta)$ using Eq. (6) above. A comparison between the measured and computed patterns is then a stringent test of the accuracy of Eq. (3). Again, it is important to note that all of these patterns functions are complex valued and that both amplitude and phase data are required to define $E_\theta(\theta)$ and $E_\phi(\theta)$ and in computing patterns using Eq. (6). This check on Eq. (3) will be made, and errors introduced by second-order deviations of the actual pattern from the assumed form Eq. (3) will be evaluated in a later section.

C. Equations To Be Used to Compute Gain

Using Eq. (3), we may rewrite the directivity Eq. (2) as

$$G = \frac{4\pi|\mathbf{E}(0,\phi)|^2}{\pi\int_0^\pi (|E_\theta(\theta)|^2 + |E_\phi(\theta)|^2)\sin\theta\, d\theta} \tag{7}$$

This is the basic equation to be used in this report. The gain value determined using this equation is dependent on two quantities: (1) the value of the field at the single point on axis $\mathbf{E}(0,\phi)$ and (2) the integral of the radiated power over the full sphere. If the true field is $\mathbf{E}(\theta,\phi)$ and the measured field (containing errors) is $\mathbf{E}'(\theta,\phi)$, we will define an error pattern $\Delta\mathbf{E}(\theta,\phi)$ by

$$\Delta\mathbf{E}(\theta,\phi) \equiv \mathbf{E}'(\theta,\phi) - \mathbf{E}(\theta,\phi) \tag{8}$$

Then by application of the version of the triangle inequality which applies to integrals (Minkowski's inequality) it may be shown that

$$1 - \left(\frac{\Delta P}{P_T}\right)^{1/2} \leq \left(\frac{P'}{P_T}\right)^{1/2} \leq 1 + \left(\frac{\Delta P}{P_T}\right)^{1/2} \tag{9}$$

where

P_T = radiated power of the true pattern

P' = radiated power of the measured pattern

ΔP = radiated power of the error pattern

The ratio P'/P_T represents the resulting error in computing the radiated power (the denominator of Eq. 7); this will be useful in determining the effect of pattern errors on computed gain.

There is one more point to be considered. It has been shown that an error is introduced in Eq. (7) if the antenna patterns are taken about an origin other than the phase center[2] of the antenna (Ref. 2). However, if the phase center is a distance r from the center of rotation, the error in gain is given by

$$\Delta G = \left(\frac{R}{R-r}\right)^2 \tag{10}$$

This correction provides a means of taking patterns at more than one center of rotation and randomizing some sources of error. This technique is also used here.

D. Summary

By taking advantage of the special form of the radiation patterns of linearly polarized circular horns, a simplified equation for computing directive gain may be obtained which requires only the principal polarization E- and H-plane pattern data. A test to verify the assumed special form has been established, and an equation has been given to correct for changes in the computed gain for centers of rotation other than the phase center.

III. Antenna Pattern Measurement System

This section describes the measurement system, which consists of (1) an antenna range and (2) a digital antenna pattern (DAP) recording system. The objective is to identify and quantitatively determine error sources in the measurement system itself.

A. The Antenna Range

The antenna range used to measure the horn patterns (Fig. 4) is part of the JPL Mesa Antenna Range facility. The horn under test on the rotator was the receiving antenna; a mechanically identical horn was used as the illuminator. The basic requirements of a range are that it be capable of alignment to conform to the desired pattern-taking geometry described in the previous section, and that interference due to noise, reflections, or any other spurious signal be minimal.

Fortunately, with one exception, geometrical alignment is not particularly critical; if the E- and H-planes are correctly aligned in all parameters within $\pm\frac{1}{2}$ deg, the errors, which tend to uniformly affect the entire pattern, will have a very small effect. The system was aligned with a theodolite and surveying level to accuracies better

[2]In this context "phase center" means a point such that a phase pattern taken about the point would be flat at $\theta = 0$. If this point is different for the E- and H-planes, then the "phase center" is taken halfway between the two points.

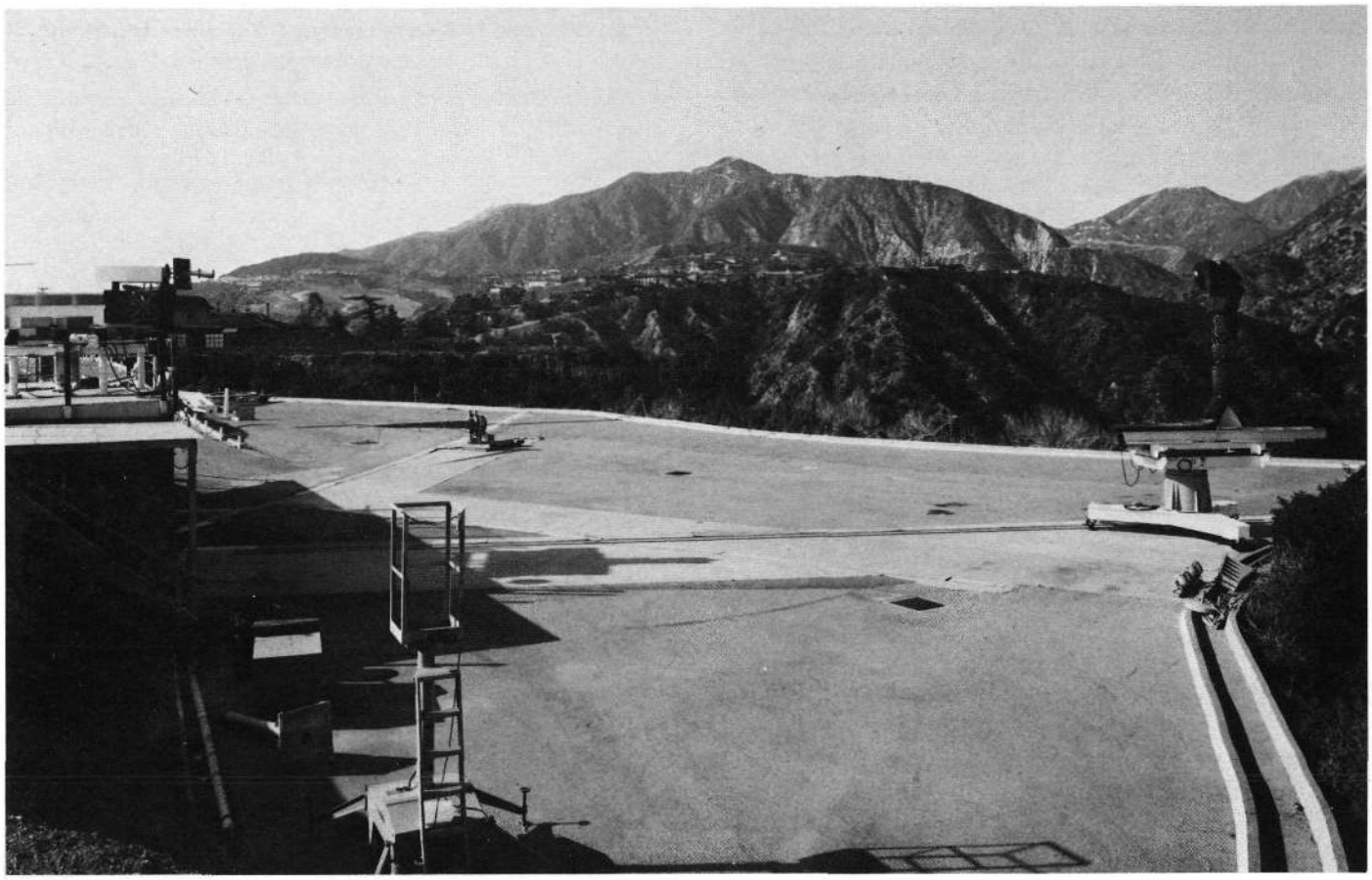

Fig. 4. Antenna range

than 0.2 deg, which will introduce negligible errors. The one exception requiring precise alignment is due to the fact that the polarization alignment is very critical for a cross-polarized pattern; an error of ½ deg would provide isolation of only −41 dB from the principal polarization component. Since cross-polarized data is not used for the gain results, this is important only for the purposes of the test of Eq. (6) to be made later. For this test, the polarization alignment was made by seeking a signal null on axis.

In addition to the alignment of the static geometry of the system, it is necessary to calibrate the one variable geometrical parameter, which is the antenna rotator angle (θ in Fig. 2). Using a theodolite as a standard, it was found that the digital angle readout was accurate to within ± 0.025 deg within ± 26 deg of boresight and ± 0.035 deg over the full ± 180-deg range. If we conservatively assume that the worst case angular errors apply systematically over the entire pattern, this leads to a maximum possible error in the calculated total radiated power of ± 0.042 dB, as shown in Table 1. It is also conservatively assumed that the error is systematic.

The range interference problem is more difficult than geometrical errors. There are several sources of interference with the antenna pattern direct signal, as shown in Fig. 5. The leakage due to sources (d), (e), and (f) illustrated in Fig. 5 was experimentally determined by covering the aperture of the receiving horn (thereby blocking the other signal paths) and then taking an otherwise normal antenna pattern. The first attempts, quite typically, showed considerable leakage into the crystal mixer on the back of the receiving horn. Careful assembly and the use of absorber finally resulted in a total worst case leakage and noise level −75 dB below the direct path maximum signal, or −52 dB below the isotropic radiated power. By Eq. (9) this would introduce a maximum gain error of ± 0.011 dB. This error will affect the pattern sets taken at different centers of rotation randomly as categorized in Table 1.

The double-bounce reflections and ground-bounce multipath may be experimentally determined by varying the separation between the transmitting and receiving

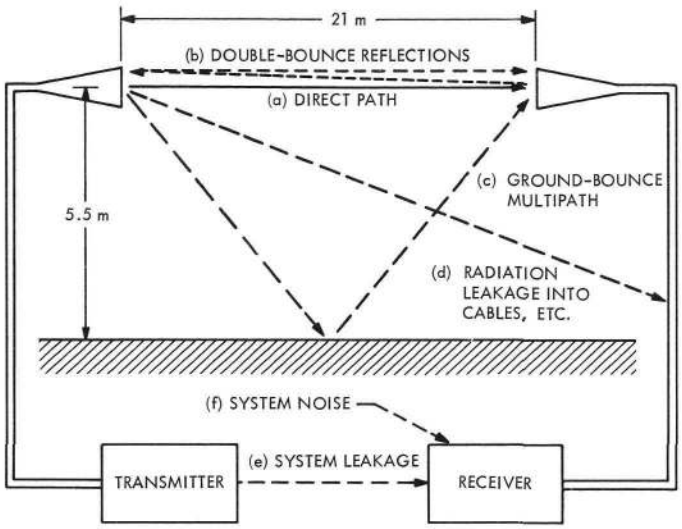

Fig. 5. Antenna range interference

horns. Leakage will also show up in this measurement, so it is quite comprehensive. Using the dimensions in Fig. 5, it may be determined that moving the horns 1.8 cm (½ wavelength) closer together will change the phase of the signal paths as follows: the direct path (a) changes by 180 deg; the double-bounce path (b) changes by 540 deg; the ground-bounce path (c) changes by 203.4 deg. Therefore, interference due to path (b) will cause a full cycle of ripple for every 1.8 cm of movement, and interference due to path (c) will cause a full cycle of ripple for every 27.7 cm of movement. The leakage path does not change in phase, so this source would cause a full cycle of ripple for every 3.6 cm of movement due to the phase change in the direct path.

The horn spacing was varied by moving the traverse table on top of the rotator at a constant speed away from the illuminating horn. The first measurement of the resulting ripple is shown in Fig. 6. The linear downward slope of the signal envelope is due to increased space loss. The fine-grain structure of the predominant interference has a peak-to-peak spacing of 1.8 cm, which indicates that it is double-bounce interference. When the transmitting and receiving masts were covered with RF absorber (Fig. 7), this ripple was greatly reduced (Fig. 8). The longer period ripple of magnitude of about ±0.01 dB has a peak-to-peak spacing of about 28 cm and therefore is positively identified as ground-bounce interference. Figure 8 shows the interference when the horns are set for an *E*-plane pattern. For an *H*-plane pattern, the ground-bounce path occurs at an angle which exactly coincides with a null in the horn pattern, so this type of interference is absent (Fig. 9).

Table 1. Gain tolerances due to antenna pattern measurement system

Source	Systematic errors, dB	Random errors, dB
DAP system angle readout errors	±0.042	–
Leakage and system noise	–	±0.011
Reflections	–	±0.03
DAP system amplitude linearity	+0.059 −0.051	–
Drift	–	±0.011
RSS total	+0.072 −0.066	±0.034

These measurements were made with the horn axis aligned. Similar interference patterns were measured with the receiving horn pointing 2, 5, 10, and 15 deg off boresight. The ripple never exceeded ±0.03 dB in any of the measured cases, which cover the first 10 dB of the horn pattern. The error that this will cause in computed gain was evaluated by actually computing the gain of two pattern sets taken at maximum and minimum interference points. This was done for the severe case, illustrated in Fig. 6, prior to the use of absorber. It was found that the peak-to-peak gain change was almost exactly equal to the peak-to-peak ripple on axis. This is less than the worst case of ±0.03 dB, but again the worst case value will be used. This error is randomized for patterns taken at different centers of rotation, and it is included in this class in Table 1.

B. The Digital Antenna Pattern Recording System

Even with the amount of data required reduced to two patterns, the pattern integration technique is not really feasible as a method of precision gain calibration without a digital pattern recording capability. The data used in this report was digitized and recorded on magnetic tape using the system diagramed in Fig. 10.

The system calibration procedure consisted of a full system RF check at 8.448 GHz using a Hewlett-Packard H382A rotary vane attenuator (Fig. 10). The rotary vane attenuator was initially calibrated using a Weinschel 1810 as part of a dual-channel insertion loss test set. The attenuator dial settings were found to be repeatable to 0.02 dB from 0 to −10 dB and 0.1 dB from −10 to −40 dB. The results of the DAP system calibration are

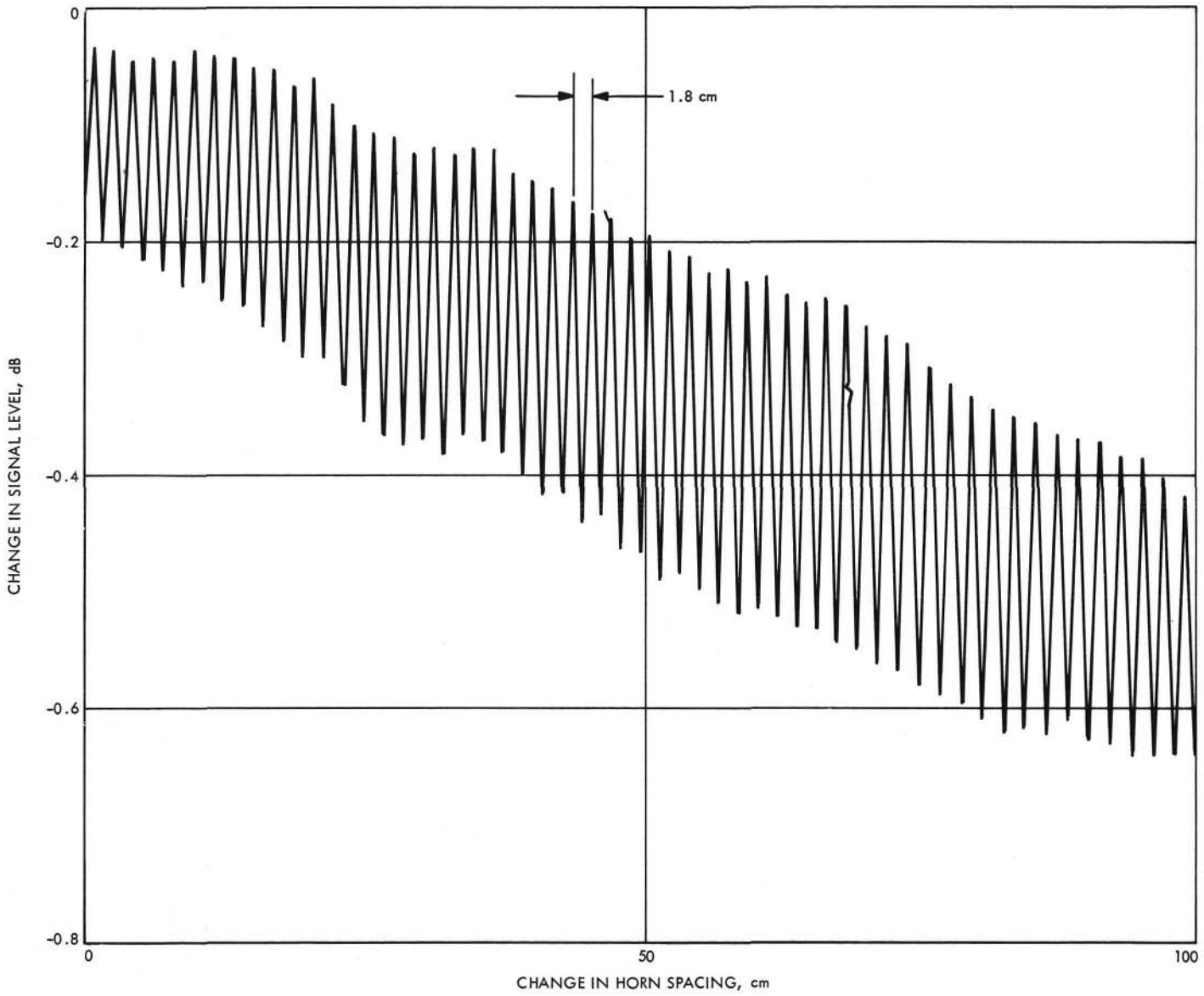

Fig. 6. Interference ripple, E-plane, initial measurement

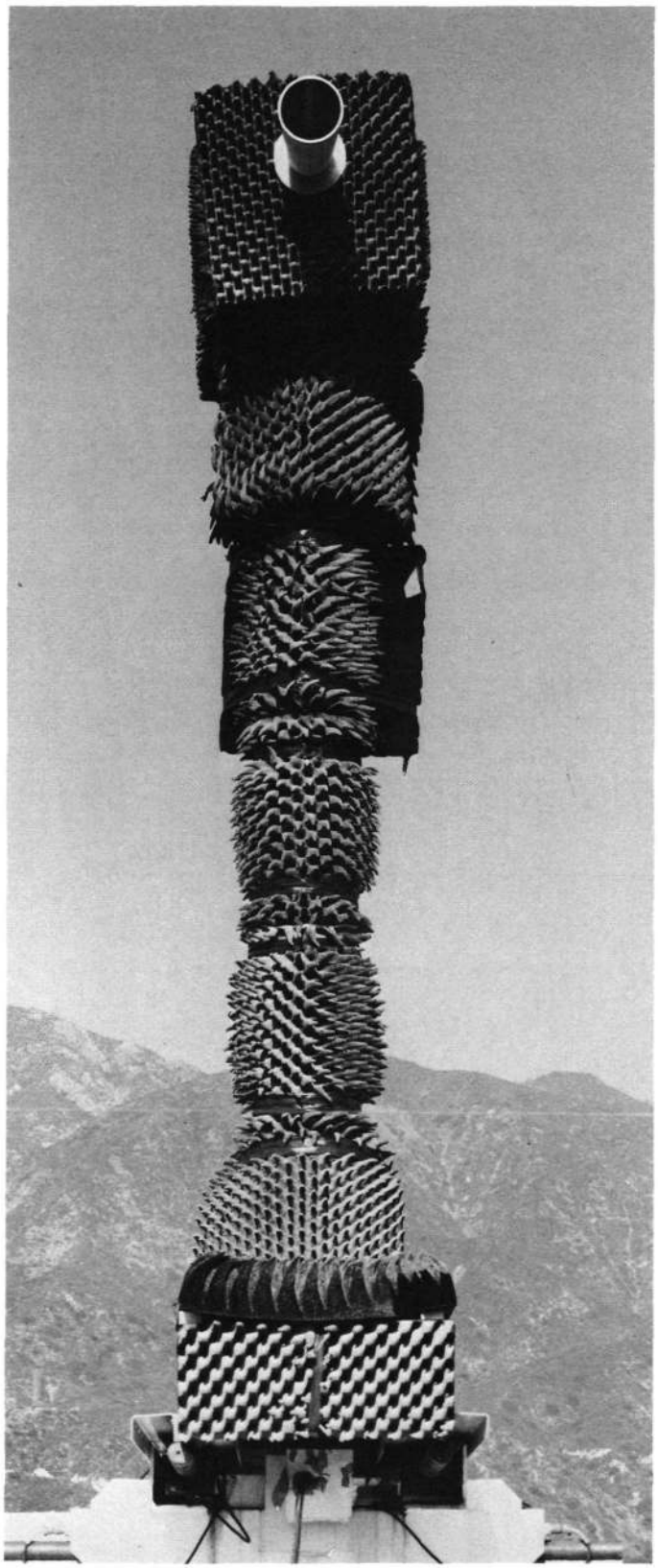

Fig. 7. Use of absorber to reduce double-bounce reflections

Table 2. Radiated power distribution in the antenna pattern

Power range, dB	Fractional power	Tolerance, dB	Maximum fractional power error
0 to −3	0.4567	±0.02	±0.0021
−3 to −10	0.1838	+0.02 −0.05	+0.0008 −0.0021
−10 to −30	0.3448	±0.10	+0.0080 −0.0078
−30 to −40	0.0122	+0.10 −0.35	+0.0003 −0.0009
Below −40	0.0025	±1.0	+0.0006 −0.0005
Totals	1.0000		+0.0118 −0.0134

given in Fig. 11 for calibrations before and after pattern data was recorded. Except for the one point at −40 dB, the agreement is very near the resolution limits of the calibration.

A test for the receiving system linearity which avoids the problem of dial setting repeatability had been made previously (Ref. 9) as follows: (1) a normal set of data is recorded; (2) the signal source power is reduced 10 dB and the digitizing and recording subsystem gain increased by 10 dB. The recorded results differed by less than ±0.025 dB in the 0–10 dB range and ±0.10 dB in the 10–40 dB range. This test does not check the linearity of the digitizing and recording subsystem; the linearity was checked separately by using a Scientific-Atlanta test set as shown in Fig. 10 and was found to be accurate to ±0.03 dB in the 0–10 dB range and ±0.14 dB in the 10–40 dB range. These prior results are generally compatible with the rotary vane attenuator calibration in spite of the dial setting error; therefore, the rotary vane calibration, which was done at the same time the pattern data was recorded, is accepted as a valid calibration for this data.

To evaluate the effect on computed gain, the error was bracketed as shown by the shaded area in Fig. 11. The fraction of the total radiated power in each of several dB ranges was determined as shown in Table 2; the appropriate tolerance for each region was then applied to obtain the overall maximum power tolerance, as given in Table 2. This power tolerance corresponds to the computed gain tolerance of $\frac{+0.059}{-0.051}$ dB shown in Table 1.

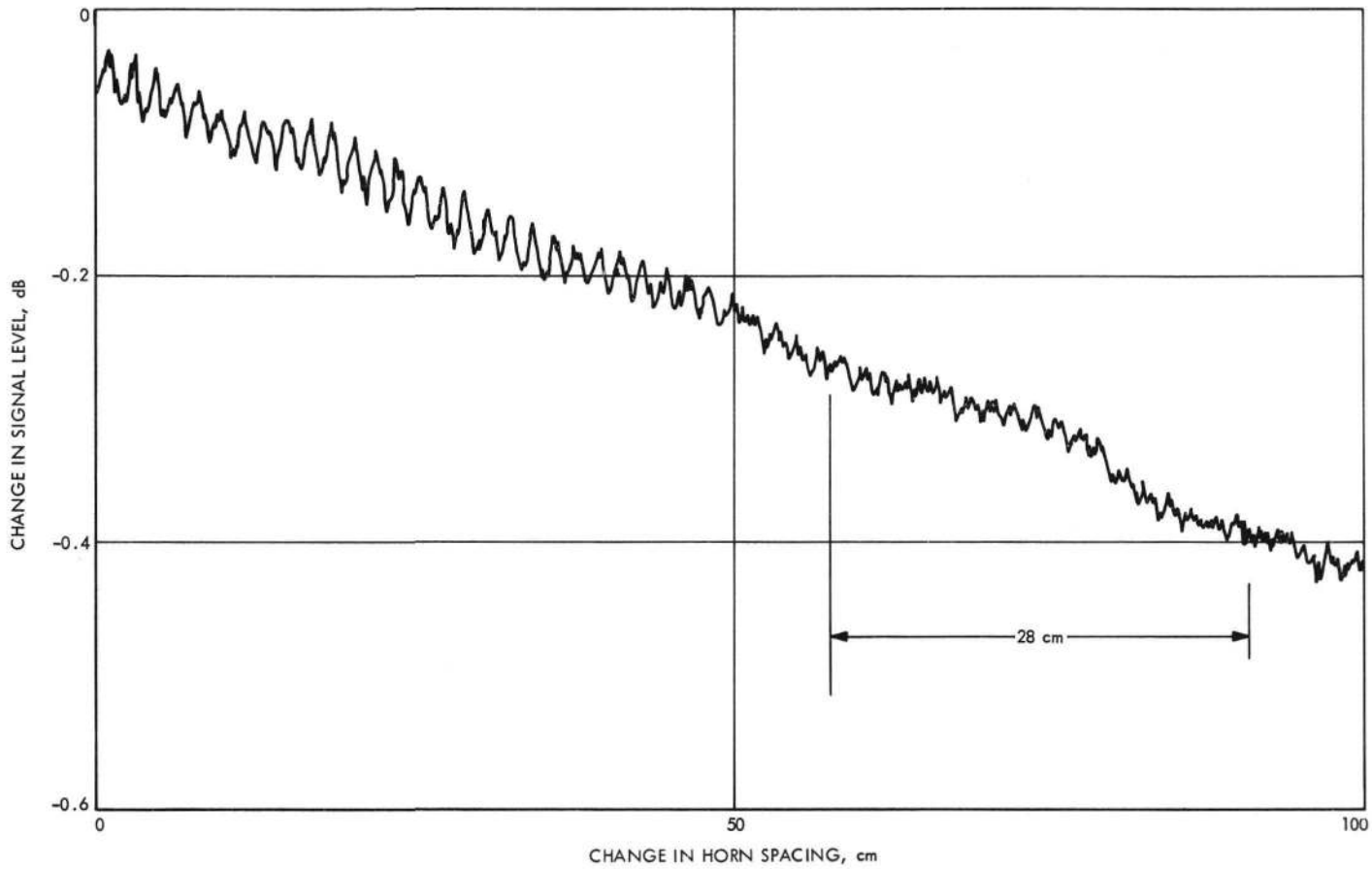

Fig. 8. Interference ripple with RF absorber, E-plane

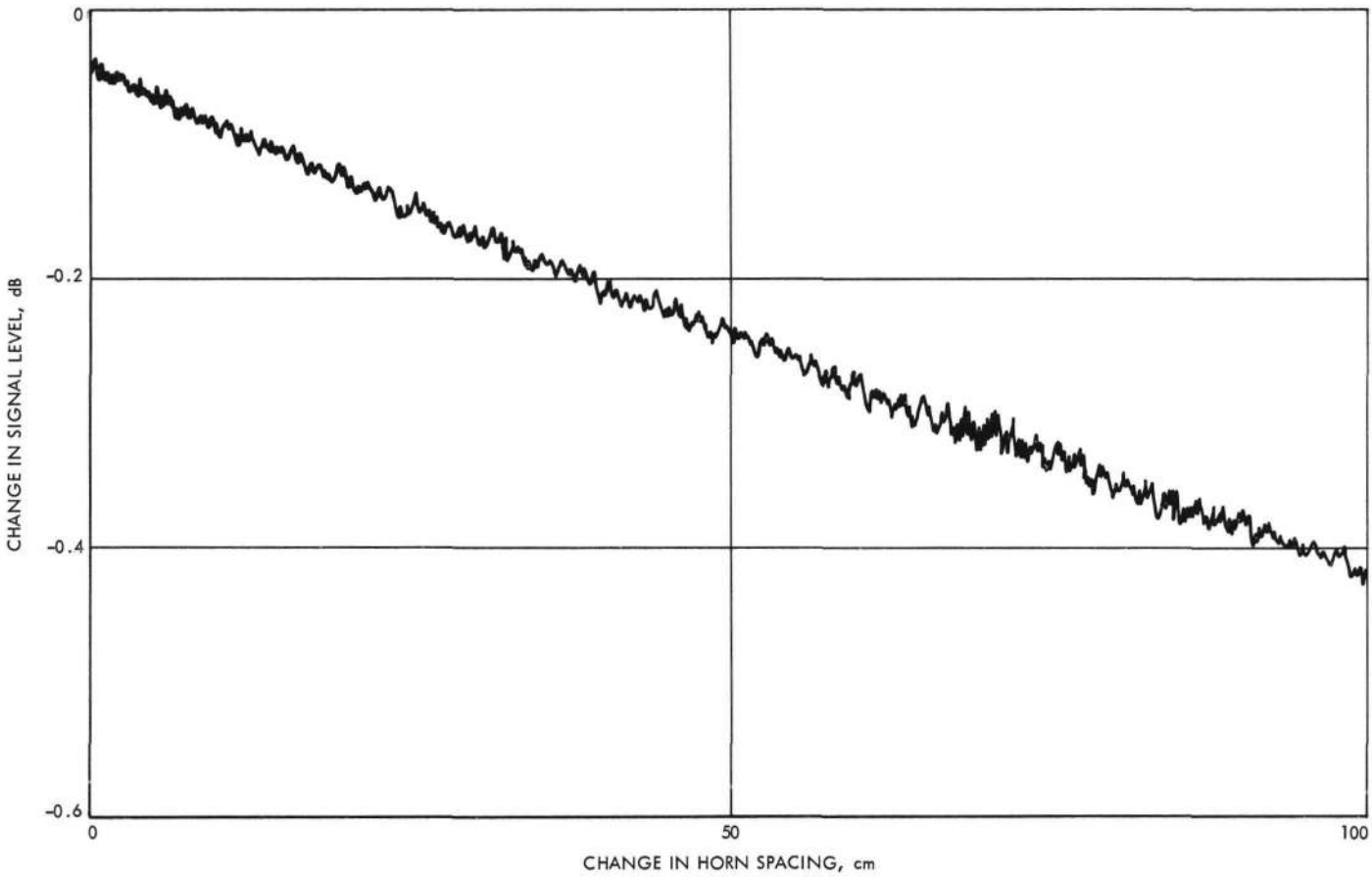

Fig. 9. Interference ripple with RF absorber, H-plane

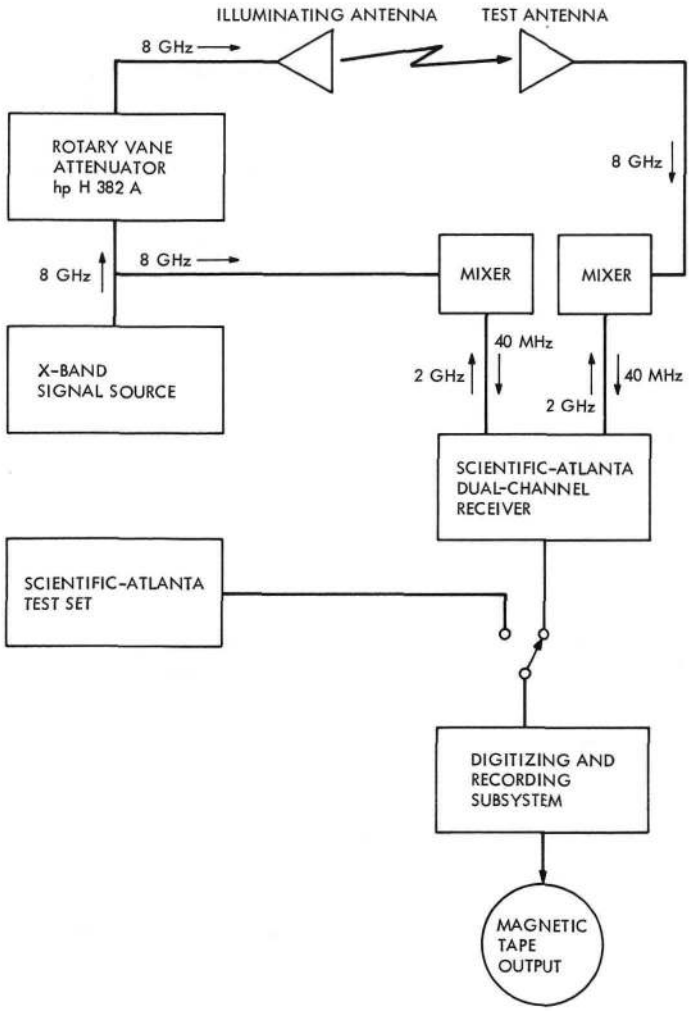

Fig. 10. Digital antenna pattern recording system

The final system test was a check on the signal stability, which will be divided into "jitter," defined as changes in signal level during a time period comparable to the data sample rate, and "drift," defined as changes in signal level during a time period comparable to measuring the pattern. The receiver is sensitive to changes in transmitted power, so this is a critical measurement. Signal changes over longer time periods between patterns are eliminated by pattern normalization. The measured maximum value of the jitter was ± 0.025 dB. The effect of this jitter on the calculated gain is significant primarily for the single data point on axis. This error will be considered in a following section on the data reduction. The measured value of drift was ± 0.04 dB over the period of time it takes to record the main beam. This occurs in a nearly linear manner over the extent of the pattern, which would result in a worst case gain error of ± 0.011 dB, as shown in Table 1.

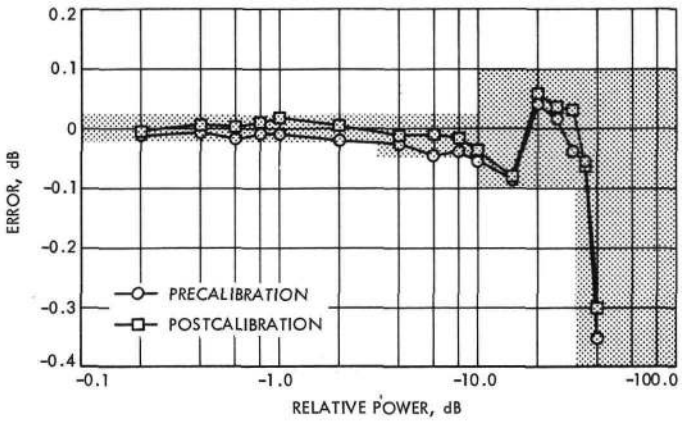

Fig. 11. Antenna recording system amplitude calibration

C. Summary

The antenna pattern measurement system introduces errors in both angular and amplitude pattern data due to system nonlinearity, noise, and interference. These errors may be quantitatively measured and fairly simple procedures used to reduce the errors due to reflection and leakage, which are otherwise severe. The resulting errors due to the various sources within the measurement system are summarized in Table 1.

IV. Pattern Measurement and Data Reduction Procedure

The experimental checks to verify that the antenna pattern is of the form of Eq. (3) are described in this section, and the data reduction procedure is considered in detail, again with emphasis on identifying sources of error.

A. Pattern Data Sets

A total of seven sets of E- and H-plane data were experimentally measured at 8.448 GHz. Since the insertion loss gain measurement made by NBS requires two horns, two nominally identical horns were available and were both used. The basic data for each horn consisted of three sets of E- and H-plane amplitude and phase patterns taken at three centers of rotation. The center of rotation is physically defined by the axis of the antenna range rotator table. The center of rotation is mathematically defined by the X-axis or Y-axis of the coordinate system (Fig. 2) for an E- or H-plane pattern, respectively. Therefore, the center of rotation can be adjusted with respect to the horn by means of the traverse table on top of the rotator. The phase center, which is defined to

be the center of rotation such that the phase pattern is flat on the beam peak, was found to be 5.398 cm behind the horn aperture. The other centers of rotation used were 60.45 cm in front of and 73.66 cm behind the phase center. In addition to these six patterns, there was a seventh phase center pattern set with the test antenna rotated 180 deg about the Z-axis, to be used in the symmetry test described below. All of these patterns are very similar to the patterns shown in Fig. 3, which happen to be phase center patterns of horn 1.

The eighth pattern set consisted of the principal and cross-polarized patterns in the $\phi = \pi/4$ plane. These were phase center patterns and are used only for the symmetry tests and not as gain calculation data.[3]

B. Experimental Verification of Pattern Symmetry

The initial objective was to verify the assumed mathematical form of the antenna pattern. There are several sources of second-order errors which could result in deviations between an actual pattern and the form of Eq. (3): (1) an elliptically polarized field rather than the assumed linear polarization, (2) physical deviations from rotational symmetry in the horn itself, and (3) reflections and other measurement errors.

An elliptically polarized field would experimentally appear as cross-polarization and will not affect the principal polarization data. Therefore, the only effect is the total power in the spurious field component. Since the spurious component will have the same pattern as the desired component, this power is found directly by measuring the polarization ellipticity or axial ratio, which was greater than 50 dB. This would introduce a systematic error in the computed power, but would cause an error in the computed gain of less than +0.00004 dB.

The method used to check the basic symmetry properties was to compute the difference between two pattern sets which should be identical; this results in an "error" pattern as defined by Eq. (8). The power in the error pattern was then computed numerically, and the maximum error this could cause in the computed gain may then be evaluated using Eq. (9). The first symmetry check was to compare the right- and left-hand sides of the same pattern. This cannot be done directly since the true pattern center is typically not precisely coincident with a sample point; however, the error power may be computed by assuming the pattern center to be at several of the closest sample points and then extrapolating the value for the true center. This rather approximate method indicates error powers more than −52 dB below the true total radiated power. This is consistent with the visually excellent symmetry of the patterns shown in Fig. 3.

The second symmetry test was to compare the patterns before and after the test antenna was rotated 180 deg about its axis (the Z axis in Fig. 2). This test also compares the right- and left-hand sides of the pattern but isolates horn effects as follows: asymmetries due to imperfections in the horn should switch sides on the pattern whereas reflections and systematic measurement errors will remain unchanged and will cancel out. In this case, the error pattern was directly computed from the raw E- and H-plane digital data. The result was error powers more than −45 dB below the true radiated power. This procedure results in an "error" pattern which is twice the actual effect. Therefore, −6 dB added to this results in an actual error power −51 dB below the true power.

The most important symmetry test is to compare the measured $\phi = \pi/4$ principal and cross-polarized patterns with patterns computed by Eq. (6). The reason that this is most significant is that it exactly simulates the way in which the symmetry is used mathematically to derive the directivity equation (7). The agreement between the computed and measured patterns was remarkable; the cross-polarized pattern is a particularly severe test since the computed principal and cross-polarized pattern is numerically the difference between the two nearly equal principal patterns (see Eq. 6). The measured and computed patterns are compared in Fig. 12, demonstrating almost unbelievable agreement. The power in the total error pattern, including both principal and cross-polarized patterns, was more than −44 dB below the true power.

These three tests are reasonably consistent and indicate a maximum error power −44 dB below the true radiated power (−66 dB below the beam peak power density). At this level it is at least as reasonable to ascribe the error power to noise effects rather than to real pattern asymmetries, but, to be conservative, it will be considered as an additional tolerance factor. Using Eq. (9), we determine that the error power of −44 dB may result in a maximum gain error of ±0.055 dB. This error and the error due to elliptical polarization are considered systematic errors, as shown in Table 3.

[3]Actually, the $\phi = \pi/4$ principal and cross-polarized patterns are also sufficient to totally define the pattern and can be used by themselves to yield the gain. This may be seen by inspection of Eqs. (3) and (6).

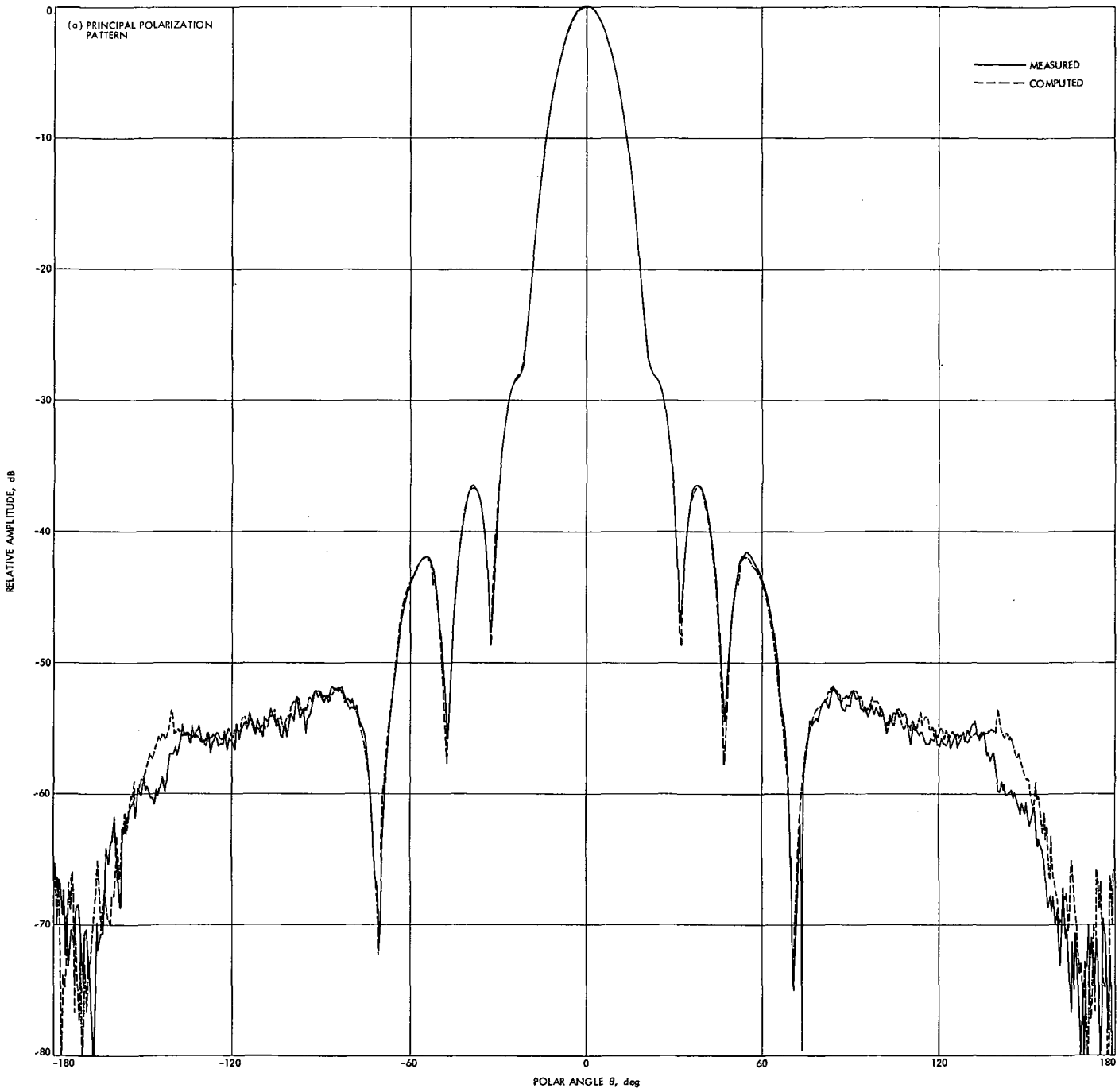

Fig. 12. Computed and measured $\phi = \pi/4$ patterns

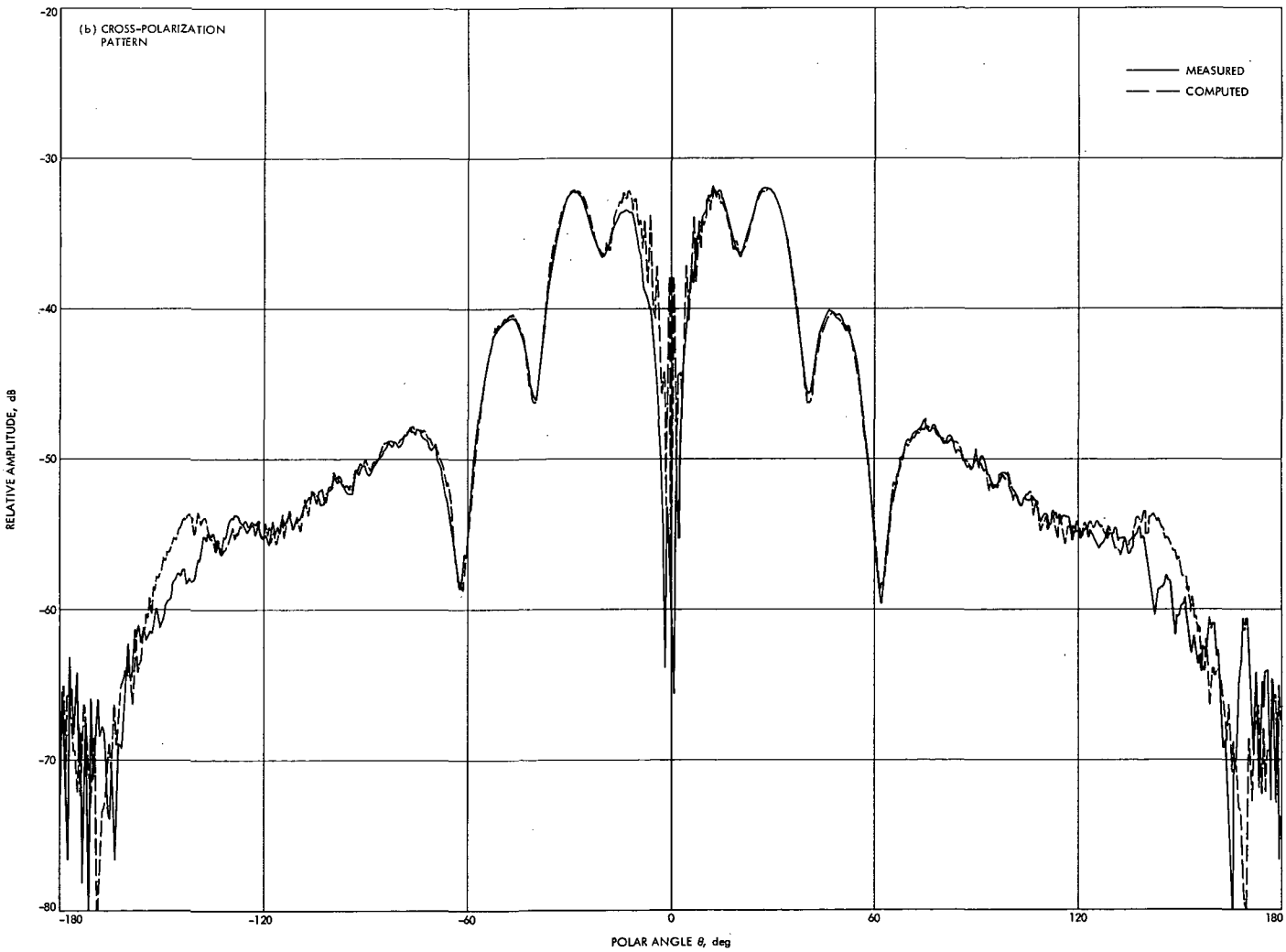
(b) CROSS-POLARIZATION PATTERN
MEASURED
COMPUTED
-20
-30
-40
-50
-60
-70
-80
RELATIVE AMPLITUDE, dB
-180
-120
-60
0
60
120
180
POLAR ANGLE θ, deg

Fig. 12 (contd)

Table 3. Gain tolerances due to pattern asymmetries and data reduction

Source	Systematic errors, dB	Random errors, dB
Elliptical polarization	+0.00004 −0.00000	–
Pattern asymmetries	±0.055	–
Data reduction	±0.005	±0.024
RSS total	±0.055	±0.024

C. Data Reduction Procedure

Even though the pattern asymmetries are slight, the first step in the data reduction was to average the right- and left-hand sides of the patterns to further reduce the effect and also to reduce the effects of jitter. To preserve the total power in the pattern, a power average is used rather than a voltage average.

$$E_{av}(\theta) \equiv \left[E^2_{right}(\theta) + E^2_{left}(\theta) \right]^{1/2} \qquad (11)$$

The phase patterns are averaged arithmetically.

If an angular error of Δ deg is made in locating the true center of the pattern, an amplitude error will be introduced by the right-left averaging process. The angular error Δ arises because the sample points for the digital data are spaced 0.5 deg apart; therefore, in the worst case Δ would be 0.25 deg. However, a reasonable alignment of the system resulted in a maximum error of $\Delta = 0.143$ deg for the patterns used in this work. To evaluate this effect, several cases were numerically investigated using the sample pattern

$$f(\theta) = e^{-k\theta^2} \qquad (12)$$

with $k = 0.006\ \text{deg}^{-2}$.

Suppose we have a perfectly symmetrical pattern $f(\theta)$ which is averaged using Eq. (11), where an error Δ deg is made in determining the center. This yields

$$f_\Delta(\theta) \equiv \left[f^2_{right}(\theta+\Delta) + f^2_{left}(\theta-\Delta) \right]^{1/2} \qquad (13)$$

The numerical cases showed that for $\Delta = 0.143$ deg, the computed gain of the pattern $f_\Delta(\theta)$ was systematically reduced by 0.002 dB relative to the computed gain of the pattern $f(\theta)$.

The second step in the data reduction was to further minimize noise effects by a moving average defined as follows:

$$E_{mav}(\theta) = \frac{1}{4} \left[E_{av}(\theta-0.5) + 2E_{av}(\theta) + E_{av}(\theta+0.5) \right] \qquad (14)$$

where the angle increment of the new data was 1.0 deg. This also introduced some second-order effects which result in a systematic gain reduction of 0.007 dB.

The final step in the data reduction was to fit an exponential pattern, of the form Eq. (12), to the peak of the main beam. The reason for this is that the basic equation for gain, Eq. (7), directly depends on the value of the peak of the beam $\mathbf{E}(0,\phi)$. If we were to rely on a single data point, jitter in this point would directly cause an error in the computed gain. By determining the value of this one critical point by curve fitting, this noise effect is greatly reduced. Also, by fitting to the original raw data, the second-order but systematic reductions in the beam peak introduced in the first two steps are eliminated, which almost exactly cancels the gain reductions. The curve was fitted to 11 data points at the peak of the beam as shown in Fig. 13. Note that this figure, which also illustrates the effect of the two averaging processes, is a highly magnified view of the beam peak with a full amplitude scale of only 0.5 dB. These changes would be much too small to see in the full antenna pattern shown in Fig. 3. Also shown in Fig. 13 is the pattern center as determined by (1) the mean of the −10 and −20 dB points on the pattern, (2) the point which minimizes the overall rms difference between the right- and left-hand sides of the pattern, and (3) the sample point selected as the center for the data reduction procedure. This center offset, although having a minor net effect on the accuracy as shown above, causes the standard deviation σ between the exponential curve and the raw data to be somewhat higher than would be expected from the directly measured value for jitter given in a previous section. The pattern shown is also one of the worst cases and was chosen because of the obviously bad point near the peak. This illustrates exactly the type of error the curve fitting is designed to eliminate. For the seven pattern sets, the average curve fit error was 0.025 dB[4]; the expected value

[4]As noted, this is the mean square average value for seven data sets; the value of 0.030 dB shown in Fig. 13 is for the single data set illustrated.

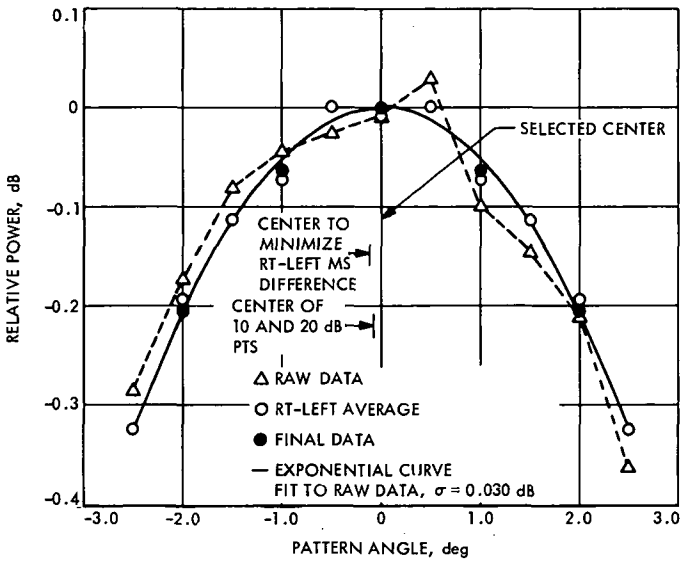

Fig. 13. Data reduction process

of the standard deviation of the peak value determined by this fit is then $0.025/\sqrt{10}$ or 0.008 dB. Even though this value is biased upwards by the offset center effect described, it will be used in place of the lower error based on the measured jitter. A 3σ value of 0.024 dB is shown in Table 3 for curve fit error, and although the other data reduction effects nominally cancel, an error of ± 0.005 dB has been included to cover any residual effects.

D. Summary

Several tests were made to verify the assumed form of the equation describing the pattern behavior and to quantitatively determine the deviations from the assumed behavior. The pattern data reduction consists of two averaging processes and a curve fit to determine the critical value at the peak of the beam. The results are summarized in Table 3.

V. Spherical Wave Expansions and Near-Field Effects

This section describes a spherical wave expansion of the horn radiation patterns which is used to compute the near-field fields of the horn. The computed near field patterns are (1) compared to NBS measured data, (2) used to evaluate errors due to near-field effects in the measured patterns, and (3) used to compute near-field correction factors for the two-horn insertion loss method of gain measurement. The first and third items above are not directly related to the main topic of this report — the pattern integration method of gain calculation — but are included because they are an interesting cross-check with the NBS results and indirectly support the main result since the spherical waves are derived from the same pattern data.

A. Spherical Wave Expansion of Horn Pattern

Spherical wave theory and techniques are described in detail elsewhere (Ref. 10) and are not repeated here. Basically, what is involved is an expansion of a radiation pattern in terms of free-space spherical waves, which are much like waveguide modes. The expansion may be evaluated to yield the fields anywhere outside a region containing the source.

The spherical wave coefficients of the horn patterns were obtained by matching the spherical wave expansion at $R = \infty$ to the experimentally measured patterns. This was accomplished using a computer program which is described in detail in Ref. 11. The input data was the final pattern data obtained as described in the preceding section.

A new test was made to determine the number of spherical waves sufficient to expand the pattern. In previous work, the total pattern power was approximated by the power in a mode expansion truncated at a very large number of modes. The actual expansion used was then truncated at a point where, for example, 99.99% of this power was contained. Figure 14 shows the fractional mode power in the first N spherical modes, where the total power is estimated by the power in the first 50 modes. Mathematically, the difference between the fractional power and the total power should exactly equal the power in the "error pattern" (see Eq. 8), defined as the vector difference between the true pattern and the truncated spherical wave expansion. However, when this error pattern power is calculated directly, a somewhat different curve is obtained (Fig. 14). The two curves begin to seriously diverge at roughly $N = 18$; this means that the spherical wave coefficients for $N >> 18$ are due as much to numerical noise as being actually present in the input pattern. Furthermore, although the total error pattern power is still slightly decreasing beyond $N = 20$, the match between the spherical wave expansion and the input pattern actually gets worse in the critical region near the peak of the beam, as discussed below. This is interesting because the maximum wave order required on theoretical grounds is approximately equal to $2\pi/\lambda$ times the radius of a sphere, centered at the origin, enclosing the aperture (Ref. 10), which, in this case, is 17.5. So it seems that the numerical noise level occurs at

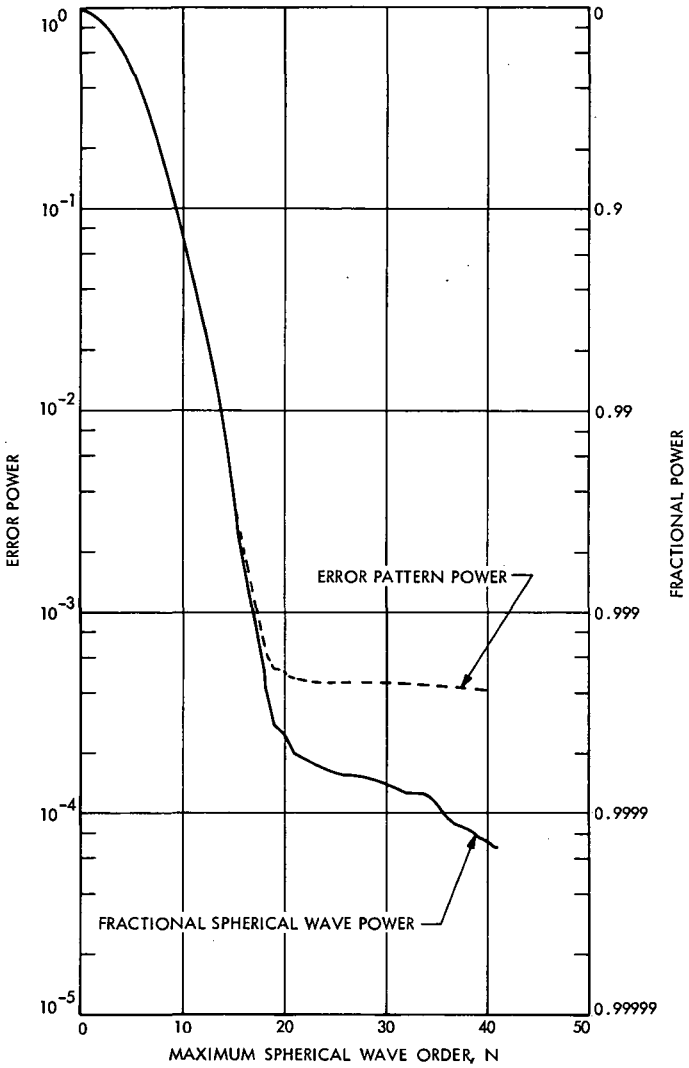

Fig. 14. Power contained in first N terms of spherical wave expansion

a value of N just above the maximum wave order expected on theoretical grounds. It is also worth noting that the error power of roughly 0.0005 is −33 dB below isotropic or about −55 dB from the pattern peak; therefore, it seems that the numerical noise is somewhat higher than the physical noise present in the measured pattern. Error power calculations restricted to the first 3 dB, 10 dB, and first null of the main beam show that the error curve bottoms out at about $N = 20$; the on-axis point on the peak of the beam is most accurate for $N = 19$ and develops significant error for $N < 16$ or $N > 22$. From this data it is concluded that the spherical wave expansion which best represents physical reality is one truncated at a value of N between 18 and 22; $N = 20$ will be selected as a nominal value.

B. Comparison of Spherical Wave Expansion and Measured Near-Field Data

As mentioned in Section I, one of the gain measurement methods being applied by NBS involves use of measured near-field data which is transformed to the far field. Here we have the inverse situation in which we can transform measured far-field data to the near field using the spherical wave expansion. This provides an outstanding opportunity to cross-compare the JPL–NBS results. To provide orientation, Fig. 15 shows a scale drawing of the JPL horn and a plane surface 20.32 cm from the horn aperture. The computed near-field fields of the horn at this plane surface are shown graphically in the same figure, where the distance from the centerline is true scale, and the amplitude is represented by the other coordinate. A more detailed graph of the same data is shown in Fig. 16. Also shown in Fig. 16 is the preliminary NBS data measured on the same plane surface (Ref. 12). The very good agreement between the data computed from the spherical wave expansion, based on JPL measured far-field patterns, and the data measured in the near-field by NBS provides strong confidence in both sets of data.

The computed data was obtained from an expansion with $N = 20$. It was found that the near-field pattern data was not particularly sensitive to the number of waves used, and was virtually identical for the cases $N = 17$, $N = 20$, and $N = 25$. Numerical checks have been made previously (Ref. 13) which show that spherical wave expansions with respect to different centers of rotation also agree very well in the near field, as long as the expansions are evaluated outside of the smallest sphere which can contain the source. Data was also obtained for two sets of horn patterns, and although the coefficients themselves differed somewhat, the final results again were virtually identical. Therefore, fortunately, these results are not particularly sensitive to either the truncation point or numerical perturbations. Since the spherical wave expansion matches experimental data in the very near field, and is forced to be equal to experimental data in the far field, there is little doubt that it is valid in between, where it will now be applied.

C. Near-Field Effects in Pattern Integration Gain Calculation

The 21-m separation between the transmitting and receiving horns shown in Fig. 5 is equal to $27.1D^2/\lambda$, where D is the horn aperture diameter. Therefore, the measurement is well beyond the conventional $2D^2/\lambda$ far-field criteria. However, when the spherical wave expansions at

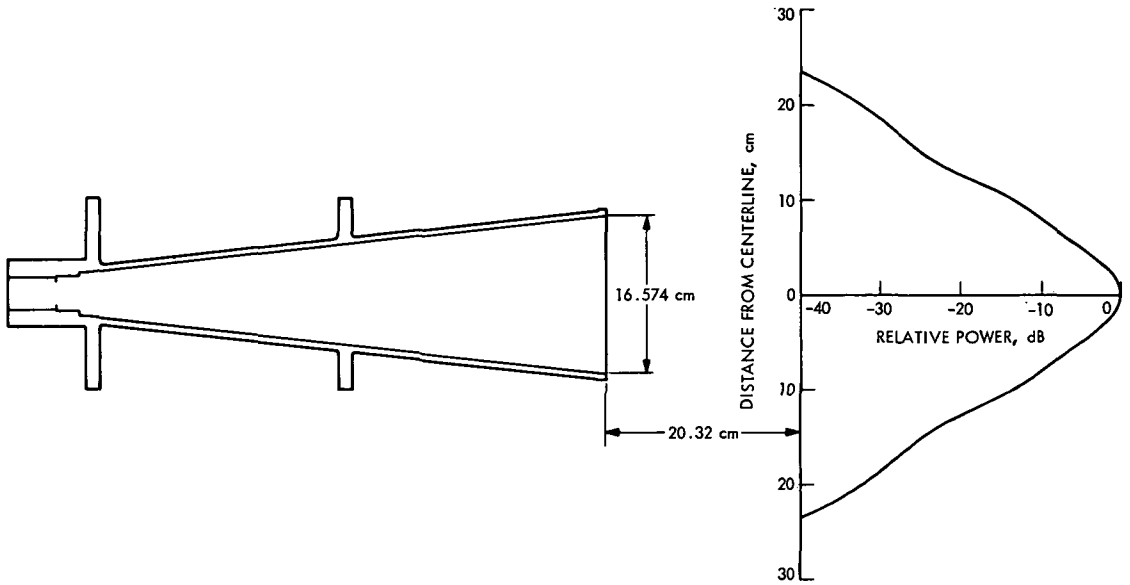

Fig. 15. Near-field pattern measurement

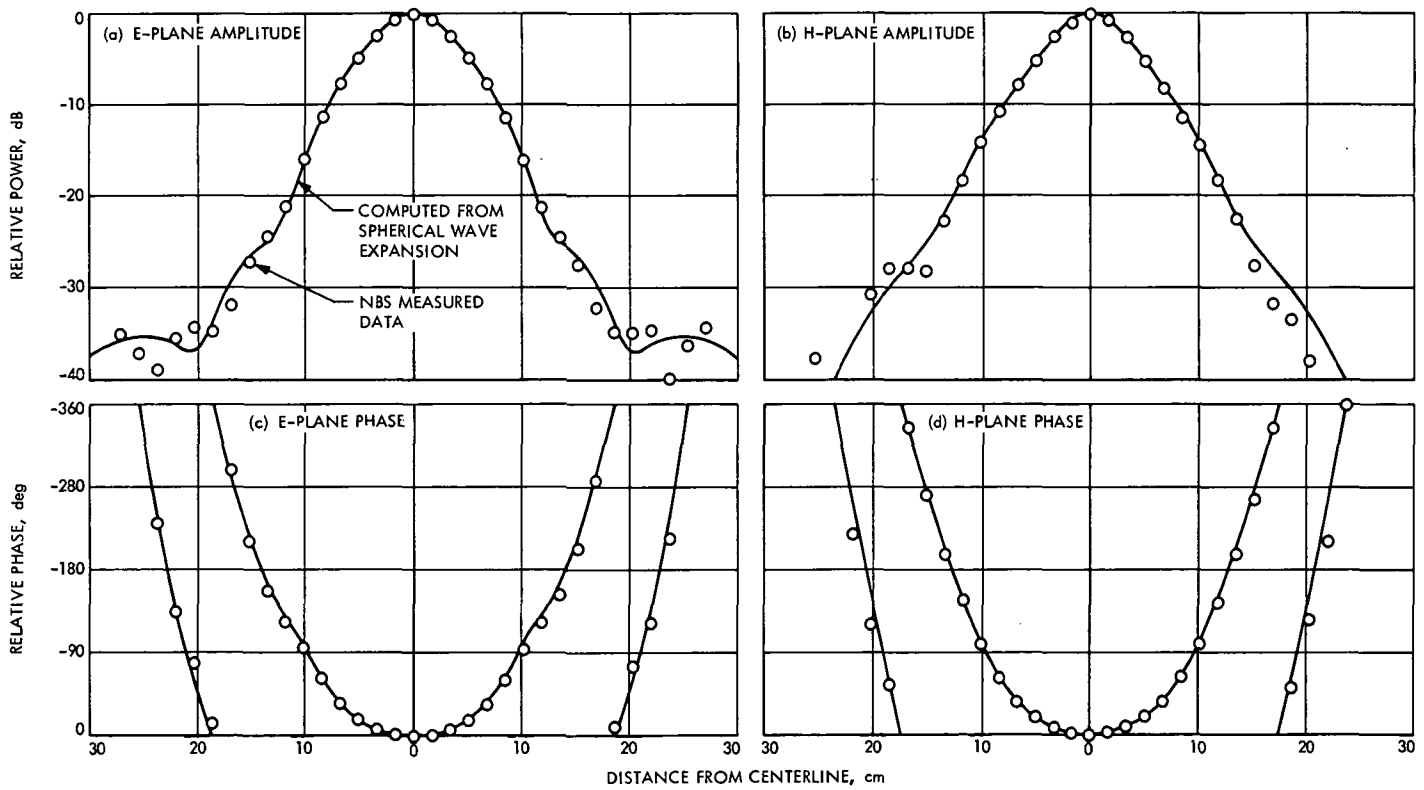

Fig. 16. Measured and computed near-field data

$R = \infty$ and $R = 21$ m were compared, it was found that the gain of the near-field pattern was 0.012 dB higher than the gain of the far-field pattern. Note that this is due to the net effect of changes in the overall pattern and not just the on-axis point. It is also important to note that this correction is for a pattern taken with the horn phase center as the center of rotation; a different result would be obtained for patterns with the center of rotation in the aperture plane, which would be incorrect in this case (Ref. 13).

It is surprising that even at this large separation, the near-field effects on the pattern are not negligible and should be included. A tolerance on the 0.012-dB correction factor is estimated to be ± 0.002 dB.

D. Near-Field Gain Correction Factors for Two-Horn Gain Measurement

When a gain is evaluated using the two-horn insertion loss method, it is essential to correct for the fact that power transfer between horns deviates from $1/R^2$ behavior in the near field because the measurement is usually in the vicinity of D^2/λ (Ref. 1). Prior methods of evaluating this correction typically involve the assumption that the fields in the transmitting horn aperture are those of the dominant mode in an infinite waveguide of similar cross section (Refs. 14, 15).

The use of the spherical wave expansion makes it possible to calculate the correction factors from the measured pattern of the horn being tested, basing the calculation firmly on experimental data instead of on a plausible but unverified assumption. The method, which has been described previously (Ref. 16), is briefly outlined here.

It has been shown (Ref. 17) that the ratio of the received to transmitted power between two antennas at any separation is

$$\frac{P_{\text{rec}}}{P_{\text{trans}}} = \frac{\frac{1}{4}\left|\int_S (\mathbf{H}_B \times \mathbf{E}_A + \mathbf{E}_B \times \mathbf{H}_A) \cdot \hat{\mathbf{n}}\, dS\right|^2}{\left[Re\int_{S_A} (\mathbf{E}_A \times \mathbf{H}_A^*) \cdot \hat{\mathbf{n}}_A\, dS\right]\left[Re\int_{S_B} (\mathbf{E}_B \times \mathbf{H}_B^*) \cdot \hat{\mathbf{n}}_B\, dS\right]} \tag{15}$$

where S_A and S_B are two closed surfaces enclosing antennas 1 and 2, respectively, $\hat{\mathbf{n}}_A$ and $\hat{\mathbf{n}}_B$ are the unit outward normals of S_A and S_B, S is a surface enclosing either one of the antennas, and $\mathbf{E}_A$, $\mathbf{H}_A$, $\mathbf{E}_B$, and $\mathbf{H}_B$ are the field quantities evaluated with both antennas in place. The quantities $\mathbf{E}_A$ and $\mathbf{H}_A$ are the fields when antenna 1 is transmitting, and $\mathbf{E}_B$ and $\mathbf{H}_B$ are the fields when antenna 2 is transmitting.

In the two-antenna insertion loss method for determining antenna gain, the ratio $P_{\text{rec}}/P_{\text{trans}}$ is measured, and the gain is calculated from

$$G(R) = \frac{4\pi R}{\lambda}\left|\frac{P_{\text{rec}}}{P_{\text{trans}}}\right|^{1/2} \tag{16}$$

where R is the separation distance between the antennas. The spherical wave expansion provides a means for directly determining the field quantities $\mathbf{E}_A$, $\mathbf{H}_A$, $\mathbf{E}_B$ and $\mathbf{H}_B$ from experimental data, which can be used in Eq. (15) to calculate the gain of an antenna as it would be measured using the two-antenna insertion loss method.[5]

Equation (15) was solved numerically on a digital computer for two identical horns at various separations. Horn-to-horn reflections were neglected; that is, $\mathbf{E}_A$ and $\mathbf{H}_A$ were calculated with horn 2 removed and $\mathbf{E}_B$ and $\mathbf{H}_B$ were calculated with horn 1 removed. With this assumption the denominator of Eq. (15) becomes the square of the total radiated power in the pattern used to compute the spherical mode coefficients. The surface S used in the numerical integration consists of a plane located midway between the horns, plus a sphere of radius $\sqrt{2}/2R$ (where R is the separation between the horns) to close the surface. This surface was chosen to maximize the numerical accuracy.

Figure 17 shows the apparent gain values as a function of the separation between the horn apertures, as measured between two identical antennas. The solid curve was obtained from an expansion derived from pattern data of horn 1; a similar expansion was obtained from pattern data of horn 2 and evaluated at the two points shown as circles in Fig. 17. It is seen that the two patterns give virtually identical results. Also, the solid curve is based on a spherical wave expansion truncated at $N = 20$. As discussed above, it was concluded that N must lie

[5]It should be noted that the near-field measurement method used by NBS provides a similar means of obtaining the quantities needed in Eq. (15) from experimental data. This method appears to be equally as good as the method used here.

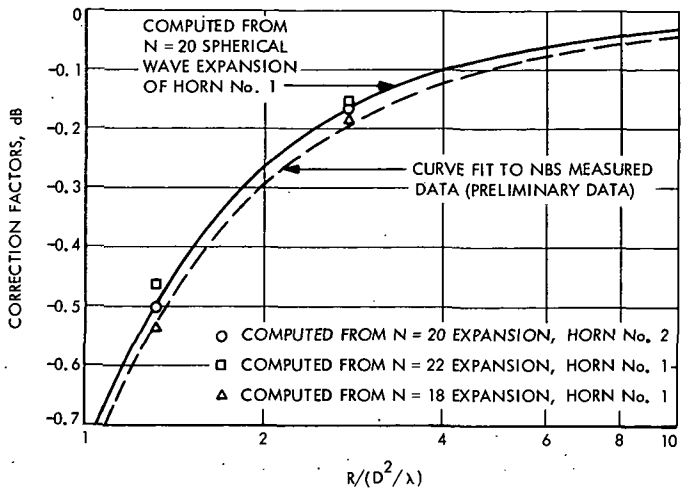

Fig. 17. Near-field gain correction factors for two-horn power transmission

between 18 and 22, so the results were spot-checked at these values. At this level of accuracy — on the order of 0.1 dB — the results are moderately sensitive to the truncation point. (This demonstrates that a careful study of the expansion errors, as described above, is necessary to insure accurate results). Also shown in Fig. 17 is a curve based on preliminary results obtained by NBS from the two horn gain experiments (Ref. 18). Again, the agreement between the independently obtained results is very good and further increases the confidence in both studies.

E. Summary

A spherical wave expansion of the horn patterns was obtained which resulted in a very low "error pattern" power. It was found that increasing the maximum wave order much above the theoretical cutoff value of 18 results in spurious waves due to numerical noise. A careful study of the error pattern between the spherical wave expansion and the input pattern led to the conclusion that the proper truncation point was between $N = 18$ and $N = 22$. The expansion was evaluated in the near field and demonstrated good agreement with NBS measured data; several numerical tests have been made which show that the near-field results are not sensitive to parameter perturbations. The spherical wave expansion was then used to evaluate near-field effects in the basic pattern data used in this report and also to determine near-field gain correction factors. The computed correction factors agree well with preliminary measured data obtained by NBS. The gain correction results are insensitive to the pattern set used but moderately sensitive to the expansion truncation point. A correction factor tolerance of ± 0.05 dB for separations of $2D^2/\lambda$ to $6D^2/\lambda$ is a reasonable estimate of uncertainty due to this effect.

Table 4. Computed gain results

Item	Apparent gain, dB	Offset r, cm	Correction ΔG, dB	Corrected gain, dB	Deviations, dB
Horn 1	22.068	0.00	0.000	22.068	0.0083
	22.361	73.66	−0.312	22.049	−0.0107
	21.814	−60.45	0.248	22.062	0.0023
	Mean corrected gain = 22.060 dB. RMS deviation = 0.008 dB.				
Horn 2	22.051	0.00	0.000	22.051	0.0055
	22.048	0.00	0.000	22.048	0.0025
	22.347	73.66	−0.312	22.035	−0.0105
	21.800	−60.45	0.248	22.048	0.0025
	Mean corrected gain = 22.046 dB. RMS deviation = 0.006 dB.				

VI. Gain Results and Error Analysis

In this section the final pattern data is used to compute the gain of the horns, which is the primary result of this work. Error data obtained for various sources in prior sections is combined into an overall error analysis for the final result.

A. Computed Gain Results

The directive gain was evaluated numerically using the final pattern data obtained as described in Section IV and Eq. (7). The results are shown as apparent gain in Table 4. As discussed, patterns were taken with the center of rotation passing through the horn phase center and also with offsets $r = -60.45$ and $r = 73.66$ with respect to the phase center; the two phase center patterns for horn 2 were a result of the 180-deg symmetry test. The apparent gain must then be corrected by factors ΔG as given by Eq. (10); these values and the mean of the corrected gain values are given in Table 4. The deviations between the corrected values and the mean and the rms deviation of the corrected values from the mean are also given in this table. It is seen that the computed gain values are very consistent, with an extremely small rms deviation of 0.008 and 0.006 dB for the two horns.

Table 5. Summary of tolerance and correction data

Source	Systematic errors, dB	Random errors, dB
DAP measurement system and antenna range	$+0.072$ -0.066	± 0.034
Pattern asymmetries and data reduction	± 0.055	± 0.024
Near-field effects	$+0.012$ ± 0.002	–
Resistive losses	$+0.021$ $^{+0.015}_{-0.005}$	–
RSS total	$+0.033$ $^{+0.092}_{-0.086}$	± 0.042

Table 6. Final gain results

Item	Gain, dB	3σ tolerance, dB
Horn 1	22.027	$^{+0.091}_{-0.097}$
Horn 2	22.013	$^{+0.089}_{-0.095}$
Average	22.02	± 0.10
NBS value	22.076	± 0.06

B. Error Analysis

The error data obtained in previous sections is summarized in Table 5. These errors are derived from peak errors, except for one case where a 3σ value (three times the standard deviation or 99.7% confidence interval for a Gaussian distribution) was used. If these are individually interpreted as 3σ values, then the rss total also represents a 3σ value (clearly the errors are independent). On this basis, the 3σ value of the calculated random errors is about twice as large as 3 times the rms scatter of the experimental data. This is felt to reflect the conservatism used in the calculated errors.

The dissipative losses in the horn, including the input section as shown in Fig. 1, have been calculated to be $0.021\ ^{+0.015}_{-0.005}$ dB (Ref. 19), as shown in Table 5.

The random errors will be reduced by a factor of $(3-1)^{1/2} = 1.4$ by the three pattern sets taken for horn 1 and by a factor of $(4-1)^{1/2} = 1.7$ by the four pattern sets taken for horn 2. Then the RSS total of the systematic errors and reduced random errors is $^{+0.097}_{-0.091}$ dB for horn 1 and $^{+0.094}_{-0.089}$ dB for horn 2. Subtracting out the systematic increase due to the near-field effects and the dissipative losses yields the final results for power gain given in Table 6. In the error analysis a positive tolerance indicates that the computed gain could be high by the given amount, so the signs on the tolerance are reversed in the final gain result. The average gain of the two horns is 22.02 dB, and the tolerance may be rounded off to ± 0.10 dB. These results are in good agreement with prior pattern integration measurements of the same horn (Refs. 2, 9), even though this earlier work did not include a comprehensive error study and suffered from the double-bounce reflection problem shown in Fig. 6. Also shown in Table 6 is the final gain value determined by NBS, which is the average of the gain of the two horns, obtained using the two-horn insertion loss method (Ref. 12).[6] The NBS result agrees with the pattern integration result within 0.056 dB. This excellent agreement between results obtained by entirely different methods gives high confidence in both methods.

VII. Conclusion

The pattern integration technique has been used to calibrate a gain standard horn with a 3σ (or 99.7% confidence) accuracy level of better than ± 0.1 dB. The average gain value determined for the two JPL standard gain horns is 22.02 dB. In addition, near-field gain correction factors for the two-horn measurement technique have been obtained with an estimated tolerance of ± 0.05 dB.

The pattern integration technique has not been developed nearly as thoroughly as the two-horn method, and it is clear that the tolerance obtained in this work, which is almost certainly conservative, could be substantially reduced. For example, there are precision rotary vane attenuators available (Ref. 20) which would enable a precise amplitude calibration of the recording system; systematic nonlinearities could then be compensated for, substantially reducing this significant source of error.

In addition to being a valuable calibration technique in itself, the pattern integration technique provides an excellent complement to other methods, both by providing a means of obtaining high-accuracy patterns for computing the two-horn correction factors and by providing a comparison of results with the near-field technique. It is felt that the method definitely deserves greater attention and use in order that it may be developed to its full potential.

[6]The result based on the near-field measurement is not yet available.

References

1. Bowman, R., "Field Strength Above 1 GHz: Measurement Procedures for Standard Antennas," *Proc. IEEE*, Vol. 55, No. 6, pp. 981–990, June 1967.

2. Ludwig, A., "Gain Computations from Pattern Integration," *IEEE Trans.*, AP-15, No. 2, pp. 309–311, Mar. 1967.

3. Baird, R. C., et al., "Recent Experimental Results in Near-Field Antenna Measurements," *Electron. Letters*, Vol. 6, No. 11, pp. 349–351, May 1970.

4. Potter, P. D., "A New Horn Antenna with Suppressed Sidelobes and Equal Beamwidths," *Microwave J.*, Vol. VI, No. 6, pp. 71–78, June 1963.

5. Bathker, D. A., et al., "High Precision Gain Standard Horn Antenna," New Technology Report 25301/NPO-11867, Jet Propulsion Laboratory, Pasadena, Calif., May 12, 1971.

6. "IEEE Standard Definitions of Terms for Antennas," *IEEE Trans.*, AP-17, No. 3, pp. 262–269, May 1969.

7. *Test Procedures for Antennas*, IEEE publication No. 149, Jan. 1965.

8. Ludwig, A., "Radiation Pattern Synthesis for Circular Horn Antennas," *IEEE Trans.*, AP-14, No. 4, pp. 434–440, July 1966.

9. Holland, R., IOM 3335-70-110 (JPL internal document), Jet Propulsion Laboratory, Pasadena, Calif., 1970.

10. Ludwig, A. C., "Near-Field–Far-Field Transformations Using Spherical Wave Expansions," *IEEE Trans.*, AP-19, No. 2, pp. 214–220, Mar. 1971.

11. Ludwig, A. C., *Calculation of Scattered Patterns from Asymmetrical Reflectors*, Technical Report 32-1430, Jet Propulsion Laboratory, Pasadena, Calif., Feb. 1970.

12. Newell, A. C., private communication, 1972.

13. Ludwig, A. C., and Norman, R., "Correction Factors for Near-Field Horn Antenna Gain Measurements," in *The Deep Space Network*, Space Programs Summary 37-57, Vol. II, pp. 104–109, May 1969.

14. Braun, E. H., "Gain of Electromagnetic Horns," *Proc. IRE*, Vol. 41, pp. 109–115, Jan. 1953.

15. Chu, T. S., and Semplak, R. A., "Gain of Electromagnetic Horns," *Bell System Tech. J.*, Vol. 44, pp. 527–537, Mar. 1965.

16. Norman, R. A., "Correction Factors for Near Field Horn Antenna Gain Measurements," in *The Deep Space Network*, Space Programs Summary 37-63, Vol. II, pp. 34-35, Jet Propulsion Laboratory, Pasadena, Calif., May 1970.

17. Hu, M. K., "Near-Zone Power Transmission Formulas," *IRE National Convention Record*, Pt. 8, pp. 128–138, 1958.

18. Bowman, R. R., private communication, May 1970.

References (contd)

19. Bathker, D., private communication, May 1971.

20. Otoshi, T., and Setlzried, C., "A Precision Compact Rotary Vane Attenuator," *IEEE Trans. Microwave Theory and Techniques*, MTT-19, No. 11, pp. 843–854, Nov. 1971.

NASA — JPL — Coml., L.A., Calif.

N72-32232

TECHNICAL REPORT STANDARD TITLE PAGE

1. Report No. 32-1572	2. Government Accession No.	3. Recipient's Catalog No.
4. Title and Subtitle GAIN CALIBRATION OF A HORN ANTENNA USING PATTERN INTEGRATION		5. Report Date October 1, 1972 6. Performing Organization Code
7. Author(s) A. Ludwig, J. Hardy, R. Norman		8. Performing Organization Report No.
9. Performing Organization Name and Address JET PROPULSION LABORATORY California Institute of Technology 4800 Oak Grove Drive Pasadena, California 91103		10. Work Unit No. 11. Contract or Grant No. NAS 7-100 13. Type of Report and Period Covered Technical Report
12. Sponsoring Agency Name and Address NATIONAL AERONAUTICS AND SPACE ADMINISTRATION Washington, D.C. 20546		14. Sponsoring Agency Code

15. Supplementary Notes

16. Abstract

A cooperative program between the Jet Propulsion Laboratory and the National Bureau of Standards will result in the gain measurement of a horn antenna using three different techniques: a two-antenna insertion loss measurement, a pattern integration method, and a near-field measurement method. This article describes the application of the pattern integration method and also the evaluation of the near-field gain correction factors for the horn, which are determined by a new method based directly on measured data. The method involves a spherical wave expansion of the experimental radiation pattern of the specific antenna being tested, rather than evaluation of an assumed analytical model. The spherical wave expansion is also compared to experimental near-field pattern data.

The gain of the antenna is determined by the pattern integration method to be 22.02 dB within a 3σ tolerance (or 99.7% confidence interval) of $\pm$ 0.1 dB. It is concluded that the pattern integration method is a valuable technique with a potential of even better accuracies with further development.

17. Key Words (Selected by Author(s))	18. Distribution Statement
Antennas and Transmission Lines	Unclassified -- Unlimited

19. Security Classif. (of this report)	20. Security Classif. (of this page)	21. No. of Pages	22. Price
Unclassified	Unclassified	26	

43725

HOW TO FILL OUT THE TECHNICAL REPORT STANDARD TITLE PAGE

Make items 1, 4, 5, 9, 12, and 13 agree with the corresponding information on the report cover. Use all capital letters for title (item 4). Leave items 2, 6, and 14 blank. Complete the remaining items as follows:

3. Recipient's Catalog No. Reserved for use by report recipients.

7. Author(s). Include corresponding information from the report cover. In addition, list the affiliation of an author if it differs from that of the performing organization.

8. Performing Organization Report No. Insert if performing organization wishes to assign this number.

10. Work Unit No. Use the agency-wide code (for example, 923-50-10-06-72), which uniquely identifies the work unit under which the work was authorized. Non-NASA performing organizations will leave this blank.

11. Insert the number of the contract or grant under which the report was prepared.

15. Supplementary Notes. Enter information not included elsewhere but useful, such as: Prepared in cooperation with... Translation of (or by)... Presented at conference of... To be published in...

16. Abstract. Include a brief (not to exceed 200 words) factual summary of the most significant information contained in the report. If possible, the abstract of a classified report should be unclassified. If the report contains a significant bibliography or literature survey, mention it here.

17. Key Words. Insert terms or short phrases selected by the author that identify the principal subjects covered in the report, and that are sufficiently specific and precise to be used for cataloging.

18. Distribution Statement. Enter one of the authorized statements used to denote releasability to the public or a limitation on dissemination for reasons other than security of defense information. Authorized statements are "Unclassified—Unlimited," "U. S. Government and Contractors only," "U. S. Government Agencies only," and "NASA and NASA Contractors only."

19. Security Classification (of report). NOTE: Reports carrying a security classification will require additional markings giving security and downgrading information as specified by the Security Requirements Checklist and the DoD Industrial Security Manual (DoD 5220.22-M).

20. Security Classification (of this page). NOTE: Because this page may be used in preparing announcements, bibliographies, and data banks, it should be unclassified if possible. If a classification is required, indicate separately the classification of the title and the abstract by following these items with either "(U)" for unclassified, or "(C)" or "(S)" as applicable for classified items.

21. No. of Pages. Insert the number of pages.

22. Price. Insert the price set by the Clearinghouse for Federal Scientific and Technical Information or the Government Printing Office, if known.